GERMAN - MONGOLIAN INSTITUTE FOR RESOURCES AND TECHNOLOGY

The present work was submitted to
the German-Mongolian Institute of Resources and Technology

KINETIC INVESTIGATION OF SPHALERITE LEACHING IN ETHALINE DEEP EUTECTIC SOLVENT

Bachelor Thesis

By

MARAL Bat-Erdene

Study program: Raw Materials and Process Engineering

Student ID: B2100336

1st Supervisor/Examiner: Dr. Purev-Ochir Togtokhbaatar

2nd Supervisor/Examiner: Prof. Gero Frisch

Advisor: Dr. Ehsan Bidari

Ulaanbaatar/Nalaikh

2025

GERMAN - MONGOLIAN INSTITUTE FOR RESOURCES AND TECHNOLOGY

The present work was submitted to
the German-Mongolian Institute of Resources and Technology

KINETIC INVESTIGATION OF SPHALERITE LEACHING IN ETHALINE DEEP EUTECTIC SOLVENT

Bachelor Thesis

By

MARAL Bat-Erdene

Study program: Raw Materials and Process Engineering

Student ID: B2100336

1st Supervisor/Examiner: Dr. Purev-Ochir Togtokhbaatar

2nd Supervisor/Examiner: Prof. Gero Frisch

Advisor: Dr. Ehsan Bidari

Ulaanbaatar/Nalaikh

2025

Statutory Declaration

Maral Bat-Erdene B2100336

I hereby affirm in lieu of an oath that I provided the submitted bachelor thesis

KINETIC INVESTIGATION OF SPHALERITE LEACHING IN ETHALINE DEEP EUTECTIC SOLVENT

I did not use any sources other than those stated. In case that the work is additionally submitted on a data medium, I declare that the written and the electronic form are completely identical. The work was not submitted in the same or similar form to any examination authority.

Ulaanbaatar, 28.05.2025 *Maral*

Place, Date Signature

ACKNOWLEDGEMENT

I would like to express my sincere gratitude to my project supervisor, Dr. Ehsan Bidari, for his exceptional guidance, continuous support, and insightful feedback throughout the course of this research. I am also profoundly thankful to Prof. Gero Frisch from the Institute of Inorganic Chemistry at TU Bergakademie Freiberg and Prof. Purev-Ochir Togtokhbaatar from the German-Mongolian Institute for Resources and Technology for their invaluable contributions and for providing me with the opportunity to expand my academic and practical knowledge in the field. Furthermore, I extend my deep appreciation to Prof. Manfred Hampe of TU Darmstadt for his academic encouragement and support, which have been instrumental in the successful completion of this work.

TABLE OF CONTENTS

LIST OF FIGURES

LIST OF TABLES

ABSTRACT

Zinc, the fourth most utilized metal after iron, aluminum, and copper, plays a vital role across a broad range of industrial sectors including metallurgy, chemical production, agriculture, and coatings. The primary source of zinc is sphalerite (ZnS), a sulfide mineral predominantly processed through pyrometallurgical and hydrometallurgical methods. However, these conventional approaches present environmental and operational drawbacks, such as high energy demands, slow kinetics, and the emission of harmful gases like SO_2. In this study, the leaching behavior of sphalerite was investigated in both aqueous and Deep Eutectic Solvent (DES) media, specifically ethaline, using $FeCl_3$ and $CuCl_2$ as oxidants. The aim was to evaluate the potential of DESs as a more sustainable and efficient leaching medium.

Experimental results showed that zinc extraction efficiency significantly depended on the solvent system, oxidant type, and temperature. The highest extraction yield (~72%) was achieved using $FeCl_3$ in ethaline at 80°C, demonstrating the effectiveness of this combination under elevated thermal conditions. Kinetic modeling using the shrinking core model indicated that diffusion-controlled leaching best fit the experimental data, particularly in $FeCl_3$ systems, where R^2 values often exceeded 0.95. However, calculated activation energies ranged from 49 to 73.5 kJ/mol, suggesting that despite the kinetic model's alignment with diffusion control, the leaching mechanism is chemically controlled in nature.

Furthermore, systems using $CuCl_2$ as the oxidant consistently exhibited higher activation energies and lower zinc extraction, implying slower reaction rates due to higher energy barriers. The superior performance of $FeCl_3$ is attributed to its strong oxidizing power, which effectively promotes sphalerite oxidation and zinc dissolution. These findings confirm the viability of DESs, especially ethaline, as an alternative leaching medium for zinc recovery from sphalerite, offering both environmental and kinetic advantages over traditional methods.

Keywords: Sphalerite, Deep Eutectic Solvents (DESs), Kinetic Analysis, Shrinking Core Model (SCM), Oxidants.

CHAPTER ONE: INTRODUCTION

Sulfide minerals represent the most important class of ore minerals and serve as the primary source for a wide range of globally significant metals (1). Among these, sphalerite is the most abundant and economically significant zinc sulfide mineral (2). Sphalerite (ZnS) and galena (PbS) are commonly found together in ore deposits, typically in varying proportions, with sphalerite usually predominating. Iron-bearing minerals, such as pyrite (FeS_2) and chalcopyrite ($CuFeS_2$), are frequently present as impurities in sphalerite deposits (3). Zinc is of particular interest not only for its industrial applications but also due to its semiconducting properties, especially its band gap, which lies within a range of suitable for diverse technological uses (4).

Zinc metal is produced through several well-established metallurgical processes, starting with the extraction of zinc from its principal ore, sphalerite (ZnS). The first step typically includes roasting, during which sphalerite is heated in the presence of oxygen to convert zinc sulfide into zinc oxide (ZnO). This is followed by smelting, a high-temperature reduction process in which zinc oxide is reduced by carbon or carbon monoxide, producing metallic zinc. Alternatively, electrowinning (a type of electrolysis) is employed, wherein an electric current is passed through an electrolyte containing dissolved zinc ions to deposit zinc metal at the cathode (5).

Pyrometallurgy processes present significant environmental challenges due to the emission of large volumes of carbon dioxide (CO_2) and sulfur dioxide (SO_2). In contrast, hydrometallurgical techniques often suffer from the slow leaching kinetics, particularly for sulfide minerals (1). Due to the inherent limitations of conventional metallurgical processes, achieveing truly “responsible consumption and production” necessitates the development of completely new approaches for metal production. A key goal is to reduce energy consumption and, therefore, CO_2 emissions by using lower reaction temperatures (6).

These limitations, combined with the increasing demand for energy-efficient, cost-effective, and environmentally sustainable extraction technologies, have led to the emergence of ionometallurgy. This innovative approach employs ionic liquids (ILs) or deep eutectic solvents (DESs) to extract metals or valuable compounds from natural ores under relatively mild conditions (7).

Ionic Liquids (ILs), per definition, are salts with a melting point below 100°C (8). DESs, on the other hand, are systems formed from a eutectic mixture of Lewis or Brønsted acids and bases which can contain a range of anionic and/or cationic species (9). While DESs share several physical properties with conventional ILs, their distinct chemical characteristics open new avenous for application (9). ILs tend to be expensive, are often non-biodegradable, and can have high toxicities, whereas DESs are generally inexpensive, biodegradable, non-toxic, and simpler to synthesize than ILs (10).

DESs offer advantages over conventional zinc extraction processes due to their excellent physical and chemical properties (9). However, a more comprehensive understanding of the leaching behavior of sphalerites in these media is required.

This study aims to enhance the understanding of the leaching behavior of sphalerite in deep eutectic solvents (DESs), particularly in Ethaline, by pursuing the following objectives:

- To obtain fundamental kinetic data through controlled leaching experiments using chloride-based DESs, Ethaline.
- To determine the kinetic parameters of sphalerite leaching in Ethaline, including the activation energy, rate constants, and the rate-controlling step, through both experimental and modeling approaches.
- To develop and propose a suitable kinetic model that accurately describes the leaching behavior of sphalerite in DES media based on the experimental findings.

CHAPTER TWO: LITERATURE REVIEW

This chapter will delve into the general properties of sphalerite, the aqueous leaching of sphalerite, and the non-aqueous leaching of sphalerite to provide relevant information necessary for the success of this research project.

2.1 General Properties of Sphalerite

A comprehensive review of sphalerite's general characteristics—including its natural occurrence, physical and crystallographic properties, processing techniques, leaching behavior, and the challenges associated with aqueous leaching—is essential, as these factors significantly impact their extraction through hydrometallurgical processes.

2.1.1 Natural occurrence of sphalerite

Sphalerite is the most common and significant zinc sulfide mineral (2). It is the fourth most widely used metal after copper, aluminum, and iron, and the twenty-fourth most common element in the earth's crust (11). Sphalerite (ZnS) and galena (PbS) commonly found together in their deposits in different proportions. However, the sphalerite usually predominates. Iron-bearing minerals, such as pyrite (FeS_2) and chalcopyrite ($CuFeS_2$), are common impurities in sphalerite deposits. On the other hand, cadmium, copper and silver, which are also often associated with sphalerite, are valuable by-products. Common gangue minerals are carbonates, such as calcite ($CaCO_3$) and dolomite ($CaMg(CO_3)_2$), quartz (SiO_2), fluorite (CaF_2) and barite ($BaSO_4$). These elements significantly influence the metallurgical performance of zinc concentrates derived from zinc ores. The extent to which sphalerite incorporates these impurities largely depends on the crystallization temperature and the composition of the ore-forming fluid. Zinc mineralization occurs at lower temperatures, common in many carbonate-hosted zinc deposits, which typically results in pale-colored sphalerite with low impurity levels. In contrast, sphalerite formed at higher temperatures is usually darker and may contain 10% or more iron. Iron content in the sphalerite increases with higher formation temperatures (3). An increase in iron content within sphalerite leads to form dark and opaque submetallic crystals known as Marmatite (3).

There are 5 major types of zinc ore deposits which is listed below:

- Sediment-hosted massive sulfides
- Volcanic-hosted massive sulfides
- Mississippi Valley Type (MVT) carbonate-hosted deposits

• Intrusion-related zinc ore deposits

• Other (3).

2.1.2 Physical properties

Sphalerite is notably characterized by its perfect cleavage in six directions, often displaying a resinous to adamantine luster on the cleavage surfaces. This property makes identification straightforward in coarse-grained specimens. However, in fine-grained samples, the cleavage can be challenging to observe, complicating visual identification (12). Sphalerite is a moderately hard mineral, with a Mohs hardness ranging from 3.5 to 4.0, and an average density between 3.9 and 4.1 g/cm³. It exhibits perfect cleavage in six crystallographic directions. The physical characteristics of sphalerite are presented in Table 1.

Table 1: Physical properties of sphalerite (13)-(14).

Property	Description
Chemical Classification	Sulfide
Color	Gray-black, yellow, red, tan, brown, black
Tenacity	Brittle
Streak	Pale yellow to brown
Luster	Nonmetallic, submetallic, resinous or adamantine
Fracture	Conchoidal
Cleavage	Perfect, dodecahedral, in six directions
Mohs Hardness	3.5 to 4
Specific Gravity (g/cm^3)	3.9 to 4.1
Crystal System	Isometric

2.1.3 Crystalline structure

Sphalerite crystallizes in the zincblende structure, a type of face-centered cubic (FCC) lattice named after the mineral itself. It is classified within the hextetrahedral crystal class, specifically in space group F43m, which is a common structure among many tetrahedrally coordinated minerals. Within this crystal structure, both the metallic cations—typically zinc and occasionally iron—and the sulfur anions are arranged in separate FCC sublattices. These sublattices are displaced relative to each other in such a way that each zinc or iron ion is tetrahedrally coordinated by four sulfur atoms, and conversely, each sulfur atom is surrounded by four metal ions. This highly symmetrical arrangement contributes to the mineral's physical properties, including its cleavage behavior and optical characteristics (15).

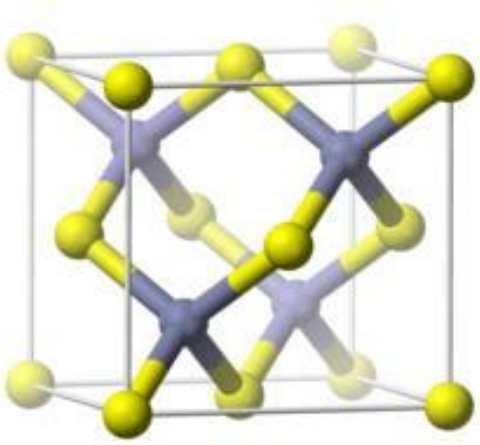

Figure 1: The crystal structure of sphalerite (15).

2.1.4 Conventional processing method of zinc

Most metals are extracted from their oxides or sulfides. These are stable compounds with low reactivity that need to be pretreated before processing. For pretreatment either high temperatures or aggressive chemicals are needed (6). Pyrometallurgy is the main treatment method for sulfide minerals and demands high energy consumption and capital costs (1). Zinc metal is produced through a series of well-established metallurgical processes, beginning with the extraction of zinc from its primary ore, sphalerite (ZnS). The initial step involves roasting, during which sphalerite is heated in the presence of oxygen to convert zinc sulfide into zinc oxide (ZnO). This is followed by smelting, a high-temperature reduction process in which zinc oxide is reacted with carbon or carbon monoxide, yielding metallic zinc. Alternatively, electrowinning (a type of electrolysis) is employed, wherein an electric current is passed through an electrolyte containing dissolved zinc ions to deposit zinc metal at the cathode. After primary extraction, the crude zinc may undergo further refining to eliminate residual impurities and achieve high purity. Refining methods include distillation, various hydrometallurgical techniques, and solvent extraction, depending on the desired end-use and quality specifications (5). Pyrometallurgy faces environmental issues regarding the production of high volumes of carbon dioxide (CO_2) and sulfur dioxide (SO_2). On the other hand, hydrometallurgical processes are generally suffering from the slow leaching rates for sulfide minerals (1). Due to the hardly conquerable limits of conventional metallurgical processes, true “responsible consumption and production” requires completely new approaches for metal production. Energy consumption and, therefore, CO_2 emissions need to be reduced by using lower reaction temperatures (6).

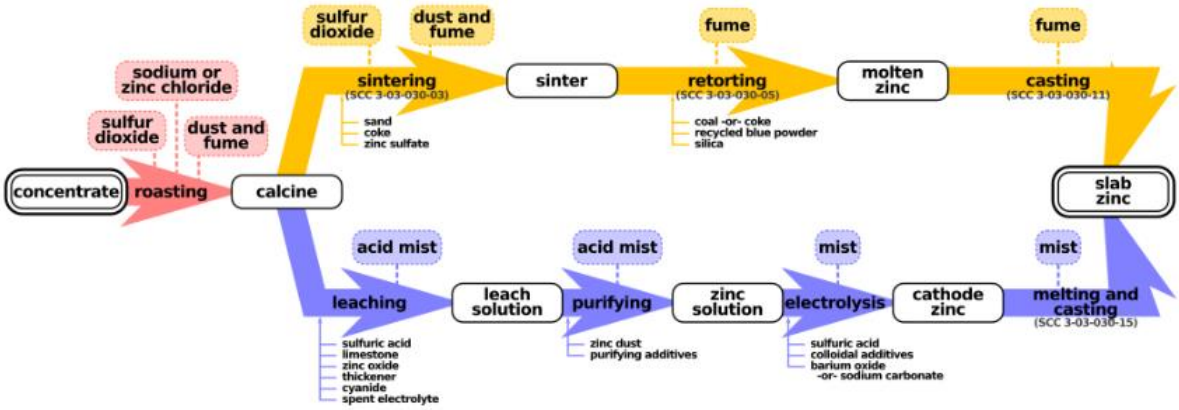

Figure 2: Conventional processing methods of zinc (16).

2.1.5 Sphalerite leaching

Numerous research studies have explored the direct leaching of sphalerite in aqueous systems under both acidic and alkaline conditions. Commonly used leaching media include ammonia solutions, nitric acid, sulfuric acid, and acidic chloride solutions. Depending on the conditions, leaching can proceed via oxidative or non-oxidative pathways. In oxidative leaching, reagents such as $FeCl_2$, $CuCl_2$, and molecular oxygen (O_2) are typically employed to enhance metal dissolution.

2.1.6 Thermodynamics

Pourbaix diagram is crucial to see thermodynamically stable phase of aqueous electrochemical system as a function of oxidation-reduction potential (Eh) and pH (17). Overall, the thermodynamic behavior of sphalerite dissolution is illustrated in the Zn–S–H_2O Eh–pH diagram (Figure 3). According to the diagram, sphalerite becomes unstable in acidic environments, resulting in the formation of Zn^{2+}(aq). As the pH increases, sphalerite dissolves only in the presence of an oxidizing agent. Zn^{2+} is dominant at low pH but gradually diminishes and eventually disappears from the system as the pH rises. This suggests that non-oxidative leaching of sphalerite is feasible in aqueous solutions under acidic conditions (18).

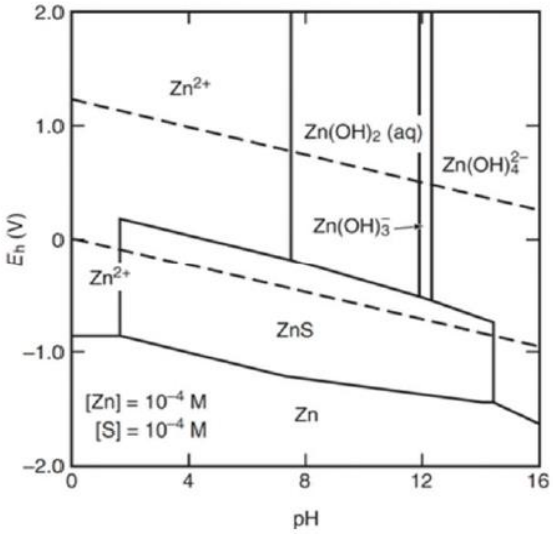

Figure 3: Eh-pH diagram for the Zn-S-H_2O system at 25°C.

2.1.7 Sphalerite leaching parameters

Sphalerite leaching in an aqueous chloride medium is affected by several parameters such as temperature, pH, viscosity, solid-to-liquid ratio, chloride concentration, concentration of reagents, stirring rate, and particle size.

- Stirring rate

  The study on the effect of stirring speed on sphalerite dissolution has been reported by several researchers (19), (2), (20), (21). Xie et al. (2007) examined the effect of stirring speed and they found that a stirring speed above 600 rpm does not affect the leaching rate. The optimum stirring rate has been identified to be between 400-600 rpm (19), (20).
- Temperature

  Temperature has a major role in the dissolution process of sphalerite. The leaching rate escalates as the temperature increases with time. Many authors have confirmed that the sphalerite dissolution increased at the elevated temperature, however, the reported values of activation energy vary widely (20), (2), (19), (21). The zinc extraction was relatively low at 40°C (45%) but significantly increased as the leaching temperature rises and a high zinc extraction at 90°C (90%) was observed by (19). Similar results were obtained by Dutrizac and MacDonald (1978), Bobeck and Su (1985), Aydogan et al. (2005), Perez and Dutrizac (1991), Dutrizac (2005), and by Babu et al. (2002) in different solutions.
- Particle size

  The influence of particle size on sphalerite leaching has been studied by several authors. Souza, Pina et al. 2007 reported that the decrease in particle size enhanced the zinc dissolution, but the role of particle size in the leaching process is considered a minor. The experiment was carried out with the particle size between 38-45 µm was only around 10% higher than the performance with the size range of 210-250 um (19). The smaller the

particle, the larger the contact surface area, resulting in faster dissolution of the sphalerite (2), (20).

- Solid-to-liquid ratio

  Sphalerite leaching rate increases with a decrease in the solid-liquid ratio (2), (20). The effect of solid/liquid ratio from 0.045 to 0.02 g/ml was investigated by them. After 150 minutes of leaching time, the result showed that the percentage of sphalerite dissolved raised from 56.8% to 86.4% (20).

- Ferric concentration

  An important factor that affects both the rate and end product of the sulfide oxidation reaction is the composition of the solution. All leaching solutions have one thing in common: they need to have an oxidant to increase the dissolution rate (2). Ferric ion is a strong oxidant used in the leaching of several metallic sulfides such as: chalcopyrite, covellite, bornite, sphalerite, etc (19). In accordance with findings by Dutrizac and MacDonald (1978), Perez et al. (1991), Aydogan et al. (2005), and Dutrizac (2005), it was evident that zinc extraction increases gradually with ferric ion concentration (19). After 6 hours of leaching with a 1.2 M concentration of ferric ions, the highest zinc recovery from the sphalerite concentrate was 84.72% at 80°C was reported by (2).

- Cupric concentration

  Cupric ions are used as oxidants for sphalerite leaching. Of the chlorides, ferric chloride, cupric chloride, sodium chloride, hydrochloric acid and elemental chlorine are most often used for oxidation (2). Dutrizac and MacDonald (1978) reported that the addition of $CuCl_2$ to the Fe(III) chloride leaching solution increased the rate of reaction (22).

- Chloride concentration

  The use of chloride systems in investigations of hydrometallurgical processing of sulfide minerals is significant. Chloride systems have several advantages over sulfate systems (2):

  1. Fe (III) chloride and Cu (II) chloride are far more aggressive than ferric sulfate.
  2. High solubility of zinc and iron.
  3. Faster oxidation of ferrous ions into ferric ions.
  4. The formation of a porous layer of sulfur that enables the diffusion of reactants to the sulfide surface.
  5. Faster leaching kinetics compared to sulfate systems.
  6. Low reactivity of pyrite in chloride systems.

2.1.8 Problems of aqueous leaching

In general, direct leaching processes can be conducted either in pressure leaching autoclaves or in agitated tanks operating under atmospheric conditions (Buban et al., 2000; Lampinen et al., 2010). Atmospheric direct leaching is considered more cost-effective than direct pressure

leaching, primarily due to lower maintenance requirements (Lampinen et al., 2015). Consequently, there has been growing interest in the application of atmospheric pressure leaching methods (Mubarok et al., 2018). However, this later is characterized by slow dissolution kinetics. The corrosive and difficult-to-regenerate solutions (acids) employed in aqueous leaching can damage equipment (23).

2.2 Introduction to Deep Eutectic Solvents

DESs are systems formed from a eutectic mixture of Lewis or Brønsted acids and bases which can contain a variety of anionic and/or cationic species. They are usually obtained by the complexation of a quaternary ammonium salt with a metal salt or hydrogen bond donor (HBD). The charge delocalization occurring through hydrogen bonding between for example a halide ion and the hydrogen-donor moiety is responsible for the decrease in the melting point of the mixture relative to the melting points of the individual components. Deep eutectic solvents can be described by the general formula Cat^+X^-zY where Cat^+ is in principle any ammonium, phosphonium, or sulfonium cation, and X is a Lewis base, generally a halide anion. The complex anionic species are formed between X^- and either a Lewis or Brønsted acid Y (z refers to the number of Y molecules that interact with the anion) (9). The solvent properties of DESs can be adjusted by changing the hydrogen-bond donor, giving 10^5 possible different liquids and making it feasible to customize the liquid's properties for particular process (24).

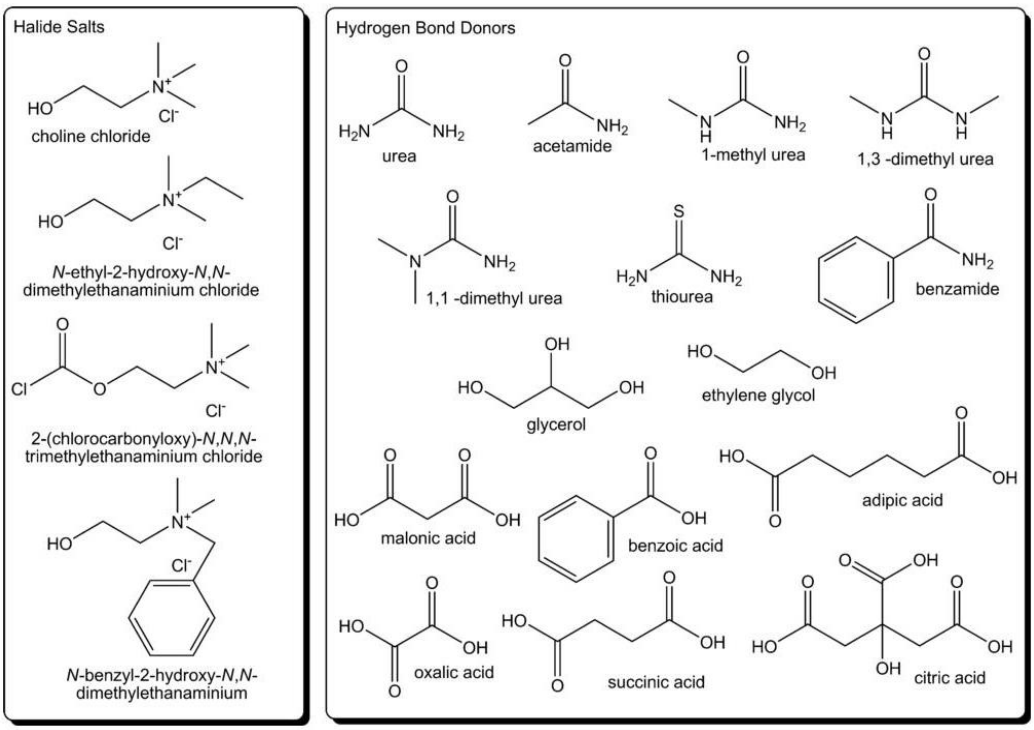

Figure 4: Structures of some halide salts and hydrogen bond donors used in the formation of deep eutectic solvents (9).

The majority of research has focused on quaternary ammonium and imidazolium cations especially in pratical systems using choline chloride, [ChCl, $HOC_2H_4N^+(CH_3)_3Cl^-$]. The main advantages of using DESs over aqueous electrolytes include their high capacity to dissolve metal salts, and superior conductivity compared to other aqueous solvents. Additionally, DESs offer broader electrochemical potential windows than aqueous systems (9). Abbott et al. called the liquid a “deep” eutectic mixture (DEM) to describe the phenomenon. These DEMs melt at sufficiently low enough temperatures to render them economically accessible as novel solvents and/or electrolytes for both emerging and established chemistries. Given that their unique properties are the main point of interest, the term “deep eutectic solvent” (DES) has become the widely accepted designation for this diverse class of materials. The wide range of properties exhibited by DESs positions them as promising alternatives to conventional molecular solvents, offering the potential for tunable optimizaztion of yield, selectivity, solubility, viscosity, cost, and other physicochemical parameters revelant to specific applications. However, due to the vast number of possible combinations of HBAs and HBDs, identifying “optimal” mixtures for a given use currently relies on impractical process of exhaustible trial-and-error across millions of potential binary systems. This challenge hinders the targeted development of DESs and undermines one of their most significant advantages, tunability, which cannot be considered a truly practical feature if the design of application-specific mixtures remains largely guesswork (10). Among these solvents, choline chloride (ChCl)-based solvents are commonly employed for metal extraction and offer superior dissolution efficiency compared to other alternatives (25).

2.2.1 Comparison with ionic liquids

Ionic Liquids (ILs), per definition, are salts with a melting point below 100°C. Typically, ILs consist of sterically demanding organic cations and organic or inorganic anions. Due to their conductivity and usually wide electrochemical windows, ILs were first considered promising electrolytes for battery or electrolysis applications (6). ILs are formed from systems composed primarily of one type of discrete anion and cation. Although the physical properties of DESs are similar to other ILs, their chemical properties suggest application areas which are significantly different (9). By the variation of cations or anions, IL properties can be tailored to fit specific applications, which, on the other hand, involve elaborate synthesis methods, making many ILs relatively expensive materials. In 2002, Abbott introduced DESs as liquids with properties similar to those of ILs, such as high conductivity, low volatility and good solubility for various materials, but with much simpler preparation. Complex organic synthesis of IL ions is replaced by the straightforward mixing of the reagents in specific ratios (6). ILs tend to be expensive, are often nonbiodegradable, and can have high toxicities, whereas DESs are typically inexpensive, biodegradable, nontoxic, and easier to prepare than ILs (7), (10).

2.2.2 Classification of DESs

DESs are traditionally classified as Type I, which combines a quaternary ammonium salt and a metal chloride, Type II, consisting of a quaternary ammonium salt and a metal chloride hydrate, Type III, consisting of a quaternary ammonium salt and a HBD, Type IV, consisting of a metal chloride hydrate and HBD, and Type V, which are a relatively new class composed of only nonionic, molecular HBAs and HBDs (10). Type I, can be considered to be of an analogous type to the well-studied metal halide/ imidazolium salt systems. Types I, II, and IV eutectics all contain metal salts with their innate toxicity; however, type III eutectics can encompass a variety of amides and polyols such as urea, glycerol, ethylene glycol, fructose, and erythritol, etc., which have low inherent toxicity (9). This research will focus on the Type III DESs, specifically Ethaline.

Table 2: General formula used for the classification of DESs (9).

Type	General formula	Terms
Type I	$Cat^+X^-zMCl_x$	M=Zn,[1,5,6] Sn,[7] Fe, Al,[8] Ga,[9] In[10]
Type II	$Cat^+X^-zMCl_x{\cdot}yH_2O$	M=Cr,[11] Co, Cu, Ni, Fe
Type III	Cat^+X^-zRZ	Z=$CONH_2$,[12] COOH,[13] OH[14]
Type IV	$MCl_x+RZ=MCl^+_{x-1}{\cdot}RZ+MCl_{x+1}$	M=Al, Zn and Z=$CONH_2$, OH

2.2.3 Type III DESs

Type III deep eutectic solvents, commonly composed of choline chloride and hydrogen bond donors, are particularly noteworthy for their ability to dissolve a wide range of transition metal compounds, including metal chlorides and oxides (9). The type III eutectic mixtures depend upon the formation of hydrogen bonds between the halide anion of the salt and the HBD; where these HBDs are multifunctional, the eutectic point tends to be toward a 1:1 molar ratio of salt and HBD. Type III DESs are known for their ability to dissolve various metal oxides (9).

2.2.4 Properties of DESs

The difference in the freezing point at the eutectic composition of a binary mixture of A + B compared to that of a theoretical ideal mixture, ΔT_f, is related to the magnitude of the interaction between A and B. The larger the interaction, the larger will be ΔT_f. This is shown schematically in Figure 2. Considering first the type I eutectics: the interactions between different metal halides and the halide anion from the quaternary ammonium salt will all produce similar halometallate species with similar enthalpies of formation. This suggests that ΔT_f values should be between 200 and 300°C. It has been observed that to produce a eutectic at about an

ambient temperature the metal halide generally needs to have a melting point of approximately 300°C or less. The same is true of the quaternary ammonium salts where it is the less symmetrical cations which have a lower melting point and therefore lead to lower melting point eutectics (9).

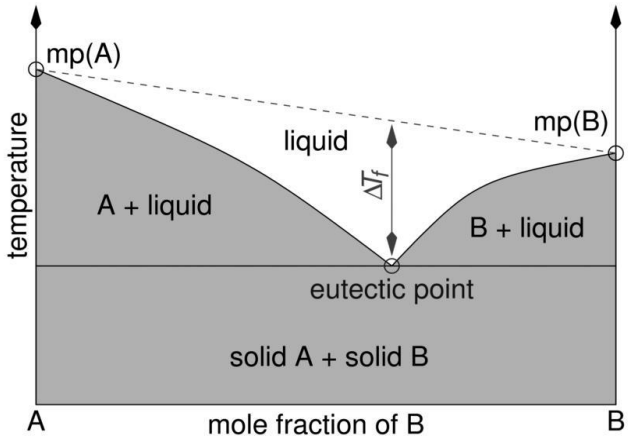

Figure 5: Schematic representation of a eutectic point on a two component phase diagram (9).

As Figure 5 shows, metal salts with lower melting points tend to produce a smaller depression of freezing point ΔT_f. This trend further illustrated in Figure 6, is attributed to the lower lattice energy of such salts, which results in weaker interactions with the chloride anion. In type III eutectic mixtures, the eutectic behavior depend on the formation of hydrogen bonds between the halide anion of the salt and the HBD; where the HBDs are multifunctional, the eutectic composition often approaches a 1:1 molar ratio between the salt and the HBD (9).

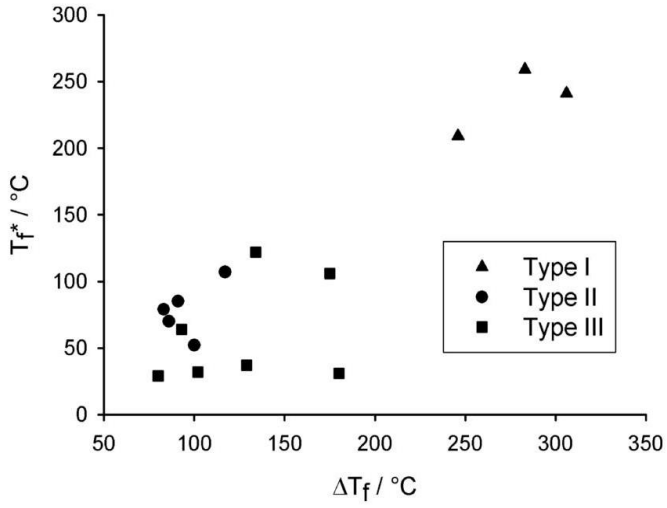

Figure 6: Correlation between the freezing temperature and the depression of freezing point for metal salts and amides when mixed with choline chloride in 2:1 ratio, where the individual points represent different mixtures (9).

2.3 Introduction to Ethaline

Ethaline is a mixture of Choline Chloride and Ethylene glycol (ChCl:EG) of molar ratio of 1:2 (24). The chemical formula of ethaline is illustrated in Figure 7. Ethaline has a low viscosity compared to the other types of DESs, making it remarkable for practical and industrial purposes. The physical properties of the Ethaline are shown in Table 3.

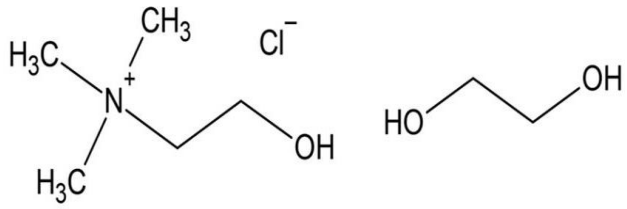

Figure 7: Chemical formula of ethaline which consists of choline chloride ($HOC_2H_4N(CH_3)_3Cl$) and ethylene glycol ($HOCH_2CH_2OH$) (26).

Table 3:Physicochemical properties of Ethaline (10).

Properties	HBA	HBD	HBA:HBD molar ratio	Reported value
Melting temperature	ChCl	EG	1:2	237 (K)
Viscosity	ChCl	EG	1:2	48 cP at 298K
Density	ChCl	EG	1:2	1.12 g/mL at 298k
pH	ChCl	EG	1:2	4.38 g/mL at 298K
Conductivity	ChCl	EG	1:2	7.63 mS/cm at 298K
Surface tension	ChCl	EG	1:2	52 mN/m at 298K
Refractive index	ChCl	EG	1:2	1.468 mN/m at 298K

CHAPTER THREE: MATERIALS AND METHODS

This chapter outlines the experimental procedures employed in this study.

3.1 Materials

3.1.1 Chemicals

Only analytical-grade reagents were utilized throughout this work. Table 4 summarizes the chemicals used and their purity.

Table 4. List of chemicals used in this study with source and purity.

Chemicals	Source	Purity %
Choline Chloride	Sigma-Aldrich	≥98%
Ethylene Glycol	Sigma-Aldrich	≥99%

3.1.2 Instruments and equipment

The feed sample was crushed using a mortar and pestle. Leach solutions were analyzed using inductively coupled plasma optical emission spectroscopy (ICP-OES), while the mineralogical characterization of the feed was performed using X-ray diffraction (XRD) machine (Bruker D8 Discover).

3.2 Methods

3.2.1 Preparation of leaching reagents

Preparation of Ethaline

Ethaline was prepared by mixing choline chloride (ChCl) and ethylene glycol (EG) in a 1:2 molar ratio. The mixture was then heated up to 323K in an oven until a clear and uniform solution was obtained. The required mass and volume calculation for ethaline from ChCl and EG were calculated and corrected for reagent purity, as shown below.

$$1 \text{ mol ChCl} : 2 \text{ mol EG}$$

$$\text{ChCl (g)} = 1 \text{ mol} \times \frac{139.62 \text{ g}}{1 \text{ mol}} \times \frac{100}{98} = 142.5 \text{ g}$$

$$\text{EG (g)} = 2 \text{ mol} \times \frac{62.07 \text{ g}}{1 \text{ mol}} \times \frac{100}{99} = 125.4 \text{ g}$$

$$\text{Total mass} = 142.5\ \text{g (ChCl)} + 125.4\ \text{g (EG)} = 267.9\ \text{g}$$

$$\text{Density of ethaline, } \rho = 1120\ \text{g/L}$$

$$\text{Volume} = \frac{267.9\ \text{g}}{1120\ \text{g/L}} = 240\ \text{ml}$$

Aqueous preparation

An aqueous solution was prepared by mixing sodium chloride (NaCl) and hydrochloric acid (HCl) in a molar ratio of 4:0.05, respectively. The prepared solution was stored in room temperature. The following calculations illustrate the quantities required to prepare 500 mL of the solution.

$$\text{Mass} = M \times V \times M_r$$

$$\text{Mass}_{NaCl} = 4\frac{\text{mol}}{\text{L}} \times 0.5\ \text{L} \times 58.44\frac{\text{g}}{\text{mol}} = 116.88\ \text{g}$$

$$M_1 \times V_1 = M_2 \times V_2$$

$$V_{HCl} = \frac{M_2 \times V_2}{M_1} = \frac{0.1\ \text{M} \times 0.5\ \text{L}}{12.08\ \text{M}} = 4.130\ \text{mL}$$

3.2.2 Feed sample preparation

The sphalerite sample, shown in Figure 8, was obtained from the Institute of Inorganic Chemistry at TU Bergakademie Freiberg and was used in this study. Solid samples were initially crushed and ground into smaller pieces, as illustrated in Figure. The ground material was then wet-sieved through 100 µm and 45 µm mesh screens, resulting in three particle size fractions: +100 µm, -100 +45 µm, and -45 µm. The separated fractions were dried in an oven at 50°C for 24 hours. All experimental procedures in this study were conducted using the -100 +45 µm particle size fraction.

Figure 8: Crushing of sphalerite mineral sample using mortar and pestle.

3.2.3 Characterization of the Feed Sample

The feed sample was characterized using X-ray diffraction (XRD), X-ray fluorescence (XRF), and inductively coupled plasma optical emission spectroscopy (ICP-OES).

X-ray diffraction (XRD) analysis

The mineralogical characterization of the feed sample was carried out using X-ray diffraction (XRD). An X-ray diffraction analysis was performed using a powder diffractometer equipped with a LYNXEYE detector. Measurements were conducted in continuous scan mode over a 2θ range of 5° to 70.01°, with a step size of 0.02°. The X-ray source was a Cu anode operating at 40 kV and 40 mA, with a Kα wavelength of 1.54060 Å. The experiment was conducted at room temperature (25 °C) using the coupled θ/2θ scan configuration. The result presented in Figure 10, reveals that the primary mineral phases present in the sample sphalerite (ZnS), galena (PbS), quartz (SiO_2) and pyrite (FeS_2). The diffraction data were interpreted by matching peak positions with standard reference patterns from the Powder Diffraction File (PDF) database. The feed sample is predominantly composed of sphalerite (ZnS), as indicated by the high-intensity peaks that align closely with PDF 05-0566. Secondary phases identified include galena (PbS, PDF 05-0592), quartz (SiO_2, PDF 86-1630), and pyrite (FeS_2, PDF 01-1295).

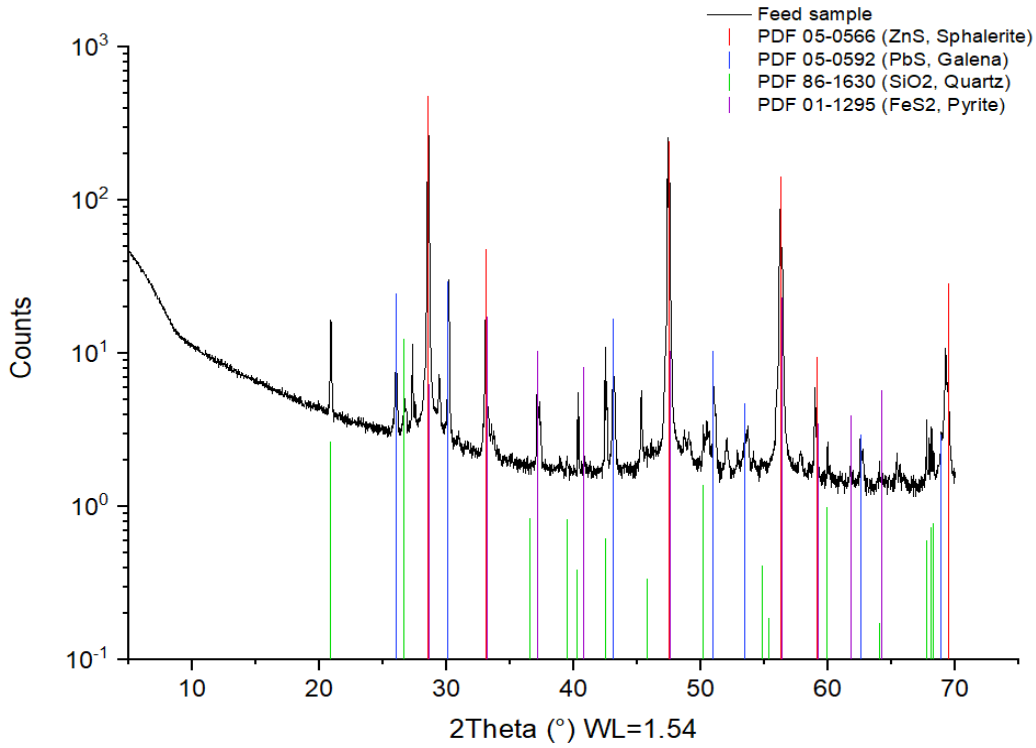

Figure 9: XRD pattern of the feed sample.

X-ray fluorescence (XRF) analysis

The chemical composition of the sphalerite sample was analyzed using X-ray fluorescence (XRF). Results were obtained in both oxide and elemental forms through the instrument's standardless quantification mode. Table 5 summarizes the oxide-based results (e.g., ZnO, Fe_2O_3), while Table 6 presents the elemental composition (e.g., Zn, Fe, S) derived from the same sample. The quantification process, specifically the way oxygen is included into oxide equivalent computations, is held responsible for small variations in concentration. To provide reliable interpretation, both oxide and elemental modes were obtained. While oxide values are used for phase identification and mineral balance, elemental percentages are useful for leaching and recovery calculations.

Table 5: Oxide-based composition (wt%) of the sample determined by XRF analysis.

No.	Oxide	Concentration (%)	Element	Notes
1	Al_2O_3	0.32%	Al	Impurity
2	SiO_2	2.54%	Si	Silicate
3	P_2O_5	0.10%	P	Impurity
4	SO_3	47.57%	S	Major component
5	MnO	0.20%	Mn	Impurity
6	Fe_2O_3	9.36%	Fe	Iron source

7	CuO	0.36%	Cu	Minor sulfide
8	ZnO	20.84%	Zn	Main component
9	Ga_2O_3	0.07%	Ga	Trace
10	ZrO_2	0.04%	Zr	Trace
11	CdO	0.19%	Cd	Trace
12	SnO_2	0.14%	Sn	Trace
13	PbO	5.08%	Pb	Minor component
14	CaO	0.12%	Ca	Trace
15	Na_2O	13.10%	Na	Possible from halite or gangue
-	Total	100.03%		

Table 6: Elemental composition (wt%) from XRF analysis.

No.	Element	Concentration (%)	Qualification method	Fitting uncertainty (%)
1	Al	0.30%	Stdless, K-line	± 0,0653
2	Si	1.85%	Stdless, K-line	± 0,0652
3	S	30.25%	Stdless, K-line	± 0,143
4	Ca	0.15%	Stdless, K-line	± 0,0195
5	Mn	0.34%	Stdless, K-line (auto)	± 0,0127
6	Fe	13.93%	Stdless, K-line (auto)	± 0,0594
7	Cu	0.68%	Stdless, K-line (auto)	± 0,0148
8	Zn	39.40%	Stdless, K-line	± 0,0910
9	Ga	0.11%	Stdless, K-line	± 0,00930
10	Zr	0.08%	Stdless, K-line	± 0,00584
11	Cd	0.45%	Stdless, K-line	± 0,00833
12	Sn	0.29%	Stdless, L-line (auto)	± 0,00727
13	Pb	12.16%	Stdless, L-line (auto)	± 0,0620
-	Total	100.09%		

Inductively coupled plasma-optical emission spectroscopy (ICP-OES) analysis

The ICP-OES analysis was performed on the sphalerite sample after digestion with a mixture of hydrogen peroxide (H_2O_2), nitric acid (HNO_3), and hydrochloric acid (HCl) under controlled condition (max. 180℃ for 10 minutes). The elemental concentration of iron (Fe), sulfur (S), and zinc (Zn) were determined. The data for the blank sample indicated that the concentrations of Fe, S, and Zn were below the detection limit, confirming the absence of significant

contamination. The sample was analyzed 3 times, and the results show a clear variation in elemental content, with zinc being the most abundant element, followed by sulfur and iron. The average concentrations of Fe, S, and Zn in the sample were 129,393 mg/kg, 265,601 mg/kg, and 357,182 mg/kg, respectively (as shown in Table 7). These values correspond to 13%, 26.6%, and 35.7% of the total mass of the sample, illustrating the high concentration of zinc in the sphalerite sample.

Table 7: Elemental composition of the sphalerite solid sample by ICP-OES.

Sample	Fe (mg/L)	S (mg/L)	Zn (mg/L)	Fe (mg/kg)	S (mg/kg)	Zn (mg/kg)
Blank	<D.L.	<D.L.	<D.L.	-	-	-
ZnS-1	60	122	164	130267	264606	356585
ZnS-2	112	228	306	133546	271179	364860
ZnS-3	93	195	262	124368	261017	350102
Average	88.36	181.54	244.07	129,393	265,601	357,182

Table 8: Average elemental composition in percentage (%).

Element	Average (mg/kg)	Percentage (%)
Fe	129,393	13
S	265,601	26.6
Zn	357,182	35.7

3.2.4 Leaching Experiments

Leaching experiments were conducted as batch processes in a glass reactor equipped with mechanical stirring at 600 rpm. A solid-to-liquid ratio of 1:100 was maintained to ensure that external mass transfer did not control the reaction rate. Experiments were performed at temperatures of 25°C, 40°C, 60° and 80°C. At designated time intervals, 2 mL of the pregnant leach solution was withdrawn, filtered, diluted with 5% nitric acid, and subsequently analyzed using ICP-OES. The sampling intervals for sphalerite conversion analysis are summarized in Table 9. To maintain a constant solution volume, an equivalent amount (2 mL) of fresh lixiviant was added after each sample withdrawal. As shown in Figure 10, the reactor setup used during the leaching process is displayed, containing the leaching solution while the reaction takes place. Table 10 provides a summary of the sample IDs and matching parameters utilized in the leaching tests.

Table 9: Sampling schedule for leaching experiments.

Experiment no.	t_0	t_1	t_2	t_3	t_4	t_5	t_6	t_7
Time	0	0.25 h	0.5 h	1 h	2 h	4 h	8 h	24 h

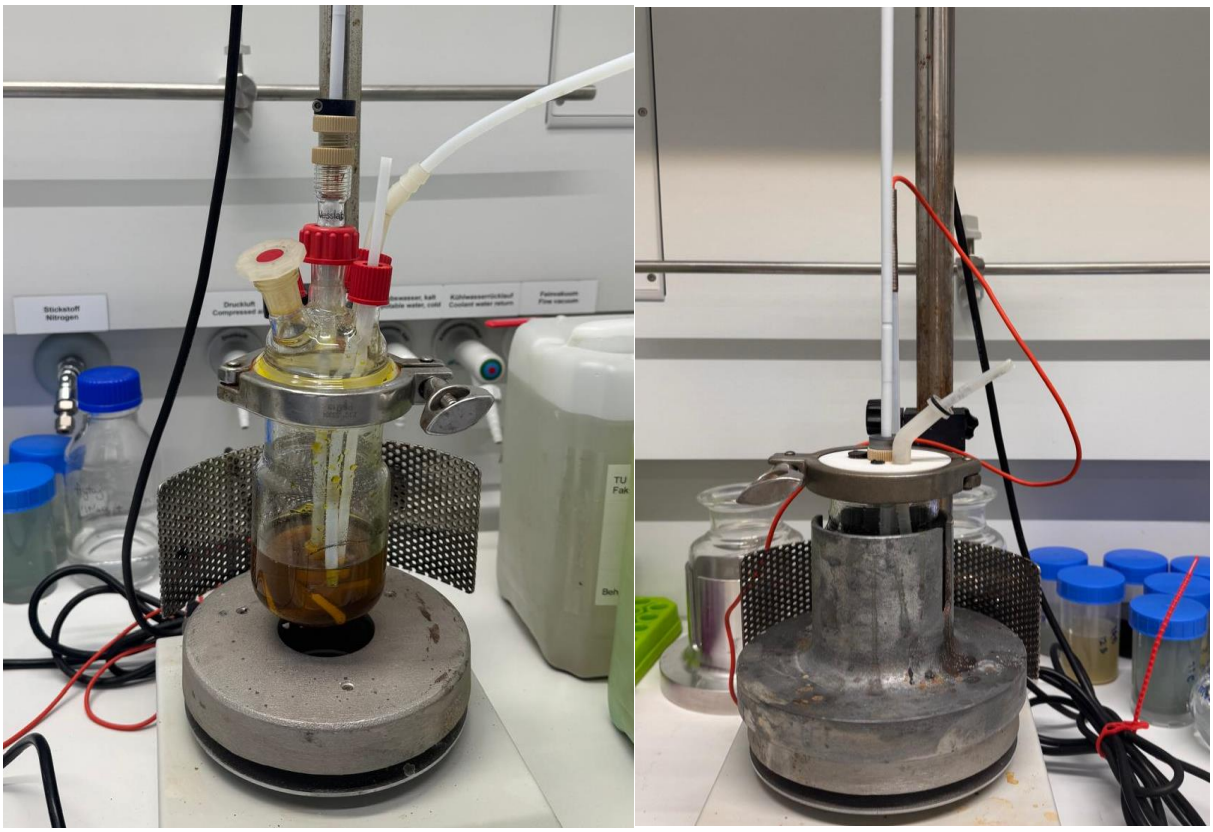

Figure 10: Reactor setup during the leaching process.

The zinc concentrations in the samples were calculated using the equation of the conversion of sphalerite:

$$X\ \%=\frac{C\times D.F}{C_o}\times 100$$

Where X is conversion, D.F is the dilution factor, C is the concentration of the zinc in the leachate (mg/L), C_o is the maximum amount of zinc that can be leached out (mg/L).

Table 10: Sample IDs and parameters used for the leaching experiment.

Sample ID	Temperature (℃)	Sample weight (g)	Volume (mL)	S/L ratio (g/L)	Stirring rate (rpm)	Particle size (µm)	Oxidants	Duration (h)	Type of solution
AF1	25	1	100	10	600	-100+45	$FeCl_3$	24	Aqueous
AC1	25	1	100	10	600	-100+45	$CuCl_2$	24	Aqueous
AF2	40	1	100	10	600	-100+45	$FeCl_3$	24	Aqueous
AC2	40	1	100	10	600	-100+45	$CuCl_2$	24	Aqueous
AF3	60	1	100	10	600	-100+45	$FeCl_3$	24	Aqueous
AC3	60	1	100	10	600	-100+45	$CuCl_2$	24	Aqueous
AF4	80	1	100	10	600	-100+45	$FeCl_3$	24	Aqueous
AC4	80	1	100	10	600	-100+45	$CuCl_2$	24	Aqueous
EF1	25	1	100	10	600	-100+45	$FeCl_3$	24	Ethaline
EC1	25	1	100	10	600	-100+45	$CuCl_2$	24	Ethaline
EF2	40	1	100	10	600	-100+45	$FeCl_3$	24	Ethaline
EC2	40	1	100	10	600	-100+45	$CuCl_2$	24	Ethaline
EF3	60	1	100	10	600	-100+45	$FeCl_3$	24	Ethaline
EC3	60	1	100	10	600	-100+45	$CuCl_2$	24	Ethaline
EF4	80	1	100	10	600	-100+45	$FeCl_3$	24	Ethaline
EC4	80	1	100	10	600	-100+45	$CuCl_2$	24	Ethaline

3.2.5 Shrinking Core Model

The shrinking core model (SCM) describes processes where solid particles undergo dissolution or chemical reaction, leading to a gradual reduction in the size of the unreacted core as the material is consumed (27). As illustrated in Figure 11, the reaction initially takes place at the outer surface of the solid particle. Over time, the reaction front progresses inward, forming a layer of fully reacted material and any inert residue—commonly referred to as "ash." Consequently, an unreacted core remains at the center of the particle, which gradually decreases in size as the reaction proceeds (28).

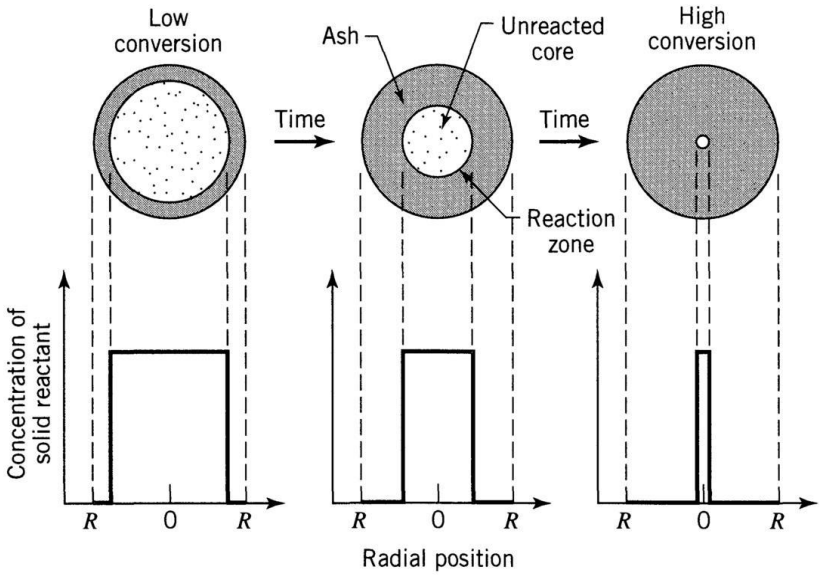

Figure 11: According to the shrinking-core model, reaction proceeds at a narrow front which moves into the solid particle. Reactant is completely converted as the front passes by (28).

Three possible rate-controlling steps for spherical particles of unchanging size are presented below with the equations:

- Diffusion Through Gas Film Controls

$$\frac{t}{\tau}=1-\left(\frac{r_c}{R}\right)^3=X$$

- Diffusion through Ash Layer Controls

$$\frac{t}{\tau}=1-3(1-X)^{\frac{2}{3}}+2(1-X)$$

- Chemical Reaction Controls

$$\frac{t}{\tau}=1-\frac{r_c}{R}=1-(1-X)^{\frac{1}{3}}$$

Conversion-time equations similar to those developed above can be obtained for various-shaped particles, and Figure 12 summarizes these expressions.

		Film Diffusion Controls	Ash Diffusion Controls	Reaction Controls
Constant Size Particles	**Flat plate** $X_B = 1 - \frac{1}{L}$ L = half thickness	$\frac{t}{\tau} = X_B$ $\tau = \frac{\rho_B L}{b k_g C_{Ag}}$	$\frac{t}{\tau} = X_B^2$ $\tau = \frac{\rho_B L^2}{2b\mathcal{D}_e C_{Ag}}$	$\frac{t}{\tau} = X_B$ $\tau = \frac{\rho_B L}{b k'' C_{Ag}}$
	Cylinder $X_B = 1 - \left(\frac{r_c}{R}\right)^2$	$\frac{t}{\tau} = X_B$ $\tau = \frac{\rho_B R}{2b k_g C_{Ag}}$	$\frac{t}{\tau} = X_B + (1 - X_B)\ln(1 - X_B)$ $\tau = \frac{\rho_B R^2}{4b\mathcal{D}_e C_{Ag}}$	$\frac{t}{\tau} = 1 - (1 - X_B)^{1/2}$ $\tau = \frac{\rho_B R}{b k'' C_{Ag}}$
	Sphere $X_B = 1 - \left(\frac{r_c}{R}\right)^3$	$\frac{t}{\tau} = X_B$ $\tau = \frac{\rho_B R}{3b k_g C_{Ag}}$	$\frac{t}{\tau} = 1 - 3(1 - X_B)^{2/3} + 2(1 - X_B)$ $\tau = \frac{\rho_B R^2}{6b\mathcal{D}_e C_{Ag}}$	$\frac{t}{\tau} = 1 - (1 - X_B)^{1/3}$ $\tau = \frac{\rho_B R}{b k'' C_{Ag}}$
Shrinking Sphere	**Small particle** Stokes regime	$\frac{t}{\tau} = 1 - (1 - X_B)^{2/3}$ $\tau = \frac{\rho_B R_0^2}{2b\mathcal{D}C_{Ag}}$	Not applicable	$\frac{t}{\tau} = 1 - (1 - X_B)^{1/3}$ $\tau = \frac{\rho_B R_0}{b k'' C_{Ag}}$
	Large particle (u = constant)	$\frac{t}{\tau} = 1 - (1 - X_B)^{1/2}$ $\tau = (\text{const})\frac{R_0^{3/2}}{C_{Ag}}$	Not applicable	$\frac{t}{\tau} = 1 - (1 - X_B)^{1/3}$ $\tau = \frac{\rho_B R}{b k'' C_{Ag}}$

Figure 12: Conversion-Time Expressions for Various Shapes of Particles, Shrinking-Core Model (28).

Data analysis can similarly reveal whether diffusion or reaction is rate controlling. If the extraction time is proportional to:

$$\left(1-\frac{2}{3}x-(1-x)^{\frac{2}{3}}\right)$$

the rate is inner diffusion controlled. If extraction time is proportional to:

$$(1-(1-x)^{\frac{1}{3}})$$

the rate is reaction controlled (29).

3.2.6 Kinetic Analysis

These models are instrumental in determining whether the leaching process is controlled by diffusion, surface chemical reactions, or a combination of both. Based on this analysis, the system's activation energy can be calculated. According to the shrinking core model, the leaching rate may be governed by the surface chemical reaction, the diffusion of reactants through the liquid boundary layer, diffusion through a solid product layer, or a combination of these mechanisms. In line with the Arrhenius equation, a system is considered diffusion-controlled when the calculated activation energy (Ea) is less than 20 kJ/mol, chemically controlled when Ea exceeds 40 kJ/mol, and mixed-controlled when Ea falls between 20 and 40 kJ/mol (30), (31).

Determination of activation energy of the leaching reactions was done by fitting the data of the leaching experiments on polynomial curve, which further evaluated to find the initial rate. The Arrhenius equation was applied to the calculation.

$$k = Ae^{\frac{-E_a}{RT}}$$

$$\ln k = \ln A + \frac{-E_a}{RT}$$

Additionally, the plot of lnk versus 1/T yields a straight line with a slope equal to –Ea/R, where Ea is the apparent activation energy of the reaction, R is the universal gas constant (8.314 J/molK), T is the temperature in Kelvin, and A is the pre-exponential factor.

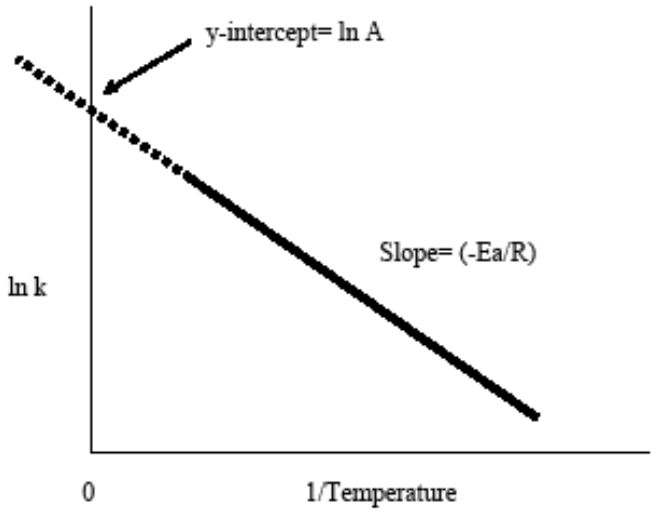

Figure 13: Arrhenius plot (32).

CHAPTER FOUR: RESULT AND DISCUSSION

This chapter will discuss the results of all the experiments undertaken for this research. This will include the sphalerite leaching in Ethaline and Aqueous media which was used as the control experiment, effect of oxidants, temperature, time and kinetic analysis of the leaching data.

4.1 Leaching Results in Ethaline DES

4.1.1 Effect of temperature on leaching

Figure 14 illustrates the effect of temperature and oxidant type on zinc extraction during the leaching of sphalerite in ethaline medium. Zinc extraction (%) is plotted against time (hours) for two oxidants, $FeCl_3$ and $CuCl_2$, at four different temperatures (25°C, 40°C, 60°C, and 80°C). The result shows that increasing the temperature significantly enhances the zinc extraction for both oxidants. At 80°C, maximum zinc dissolution (72%) is achieved, especially when $FeCl_3$ is used, while lower temperatures (25°C and 40°C) result in limited zinc recovery. The initial rate of dissolution is faster at higher temperatures, suggesting that temperature enhances both the reaction kinetics and the solubility of the reaction products. These observations confirm that elevated temperatures greatly improve the efficiency of sphalerite leaching in ethaline by accelerating the overall dissolution process.

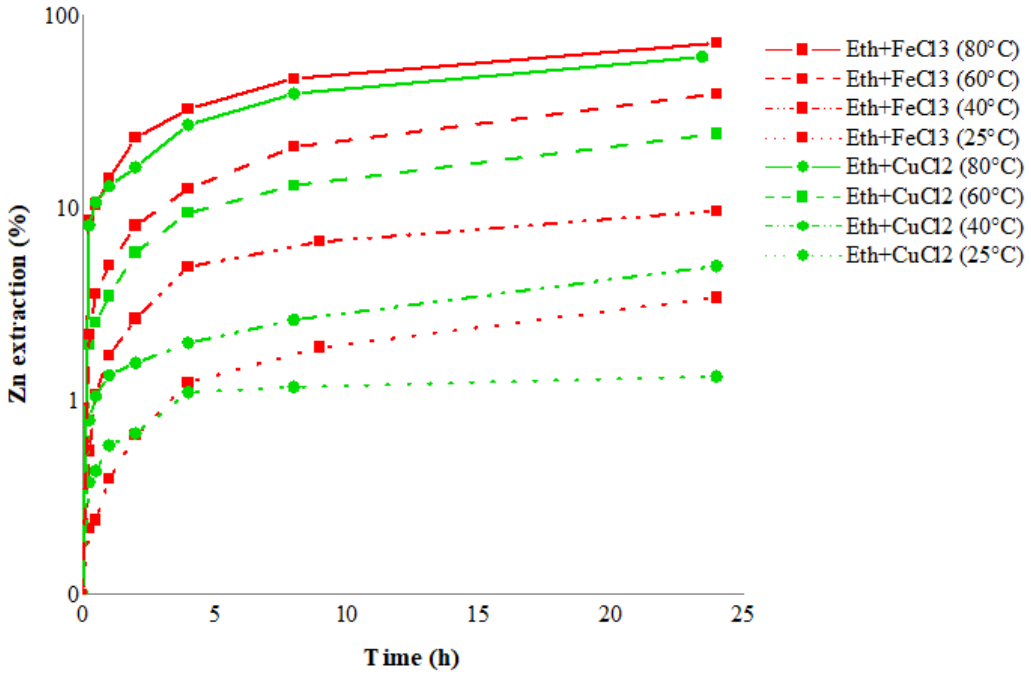

Figure 14: Effect of temperature and oxidants on zinc dissolution in ethaline.

4.1.2 Effect of oxidants on leaching

From the Figure 14, we can clearly see that the type of oxidant significantly affects zinc dissolution during sphalerite leaching in ethaline, $FeCl_3$ is notably more effective than $CuCl_2$ at all tested temperatures. Leaching with $FeCl_3$ leads to much higher zinc extraction percentages, with nearly complete dissolution at 80°C, while $CuCl_2$ results in considerably lower extraction under the same conditions. The greater efficiency of $FeCl_3$ is attributed to the higher oxidative strength of Fe^{3+} ions compared to Cu^{2+} ions in the ethaline medium. The gap in performance between the two oxidants becomes more prominent at elevated temperatures, highlighting the critical role of oxidant selection in achieving high zinc recovery.

Oxidative leaching of sphalerite is according to the equation:

$$ZnS + 2FeCl_3 + 2[Cl]^-_{DES} = [ZnCl_4]^{2-} + 2FeCl_2 + S^o$$

$$ZnS + 2CuCl_2 + 2[Cl]^-_{DES} = [ZnCl_4]^{2-} + 2CuCl + S^o$$

4.1.3 Kinetic analysis

Kinetic modeling of sphalerite leaching in Ethaline+$CuCl_2$ system

The leaching kinetics of sphalerite in ethaline with $CuCl_2$ were evaluated using shrinking core models representing both chemical reaction-controlled and diffusion-controlled mechanisms. Figure 15a illustrates the fit of the chemical reaction-controlled model $[1-(1-x)^{\frac{1}{3}}]$ plotted against time. At moderate temperatures (40–60°C), the data exhibited reasonably linear trends, with the best fit observed at 60°C (R^2=0.9497), suggesting partial chemical control in this range. However, at higher temperatures (80°C), although the slope increased-indicating an enhanced leaching rate—the R^2 value slightly decreased (0.9386), implying deviation from purely chemical control.

In contrast, the diffusion-controlled model $1-\frac{2}{3}x-(1-x)^{\frac{2}{3}}$, presented in Figure 15b, showed excellent linearity at elevated temperatures. Particularly, the 80°C dataset yielded a strong correlation (R^2=0.9984), followed by similarly high R^2 values at 60°C and 40°C (0.9968 and 0.9934, respectively). These results suggest that at higher temperatures, the rate-limiting step shifts toward the diffusion of Zn^{2+} ions through the product layer formed during leaching.

Activation energies (Ea) for both mechanisms were derived from the Arrhenius plots (Figure 15c). The Ea for the chemical reaction-controlled mechanism was calculated as 73.5 kJ/mol, while the diffusion-controlled process exhibited a higher Ea of 129.9 kJ/mol. These values indicate that both mechanisms involve considerable energy barriers, with the higher Ea for

diffusion suggesting that it becomes the rate-limiting step under high-temperature conditions. Overall, the kinetic behavior points to a temperature-dependent transition in the rate-controlling step, from surface chemical reaction at lower temperatures to diffusion control at elevated temperatures in the Ethaline+$CuCl_2$ system.

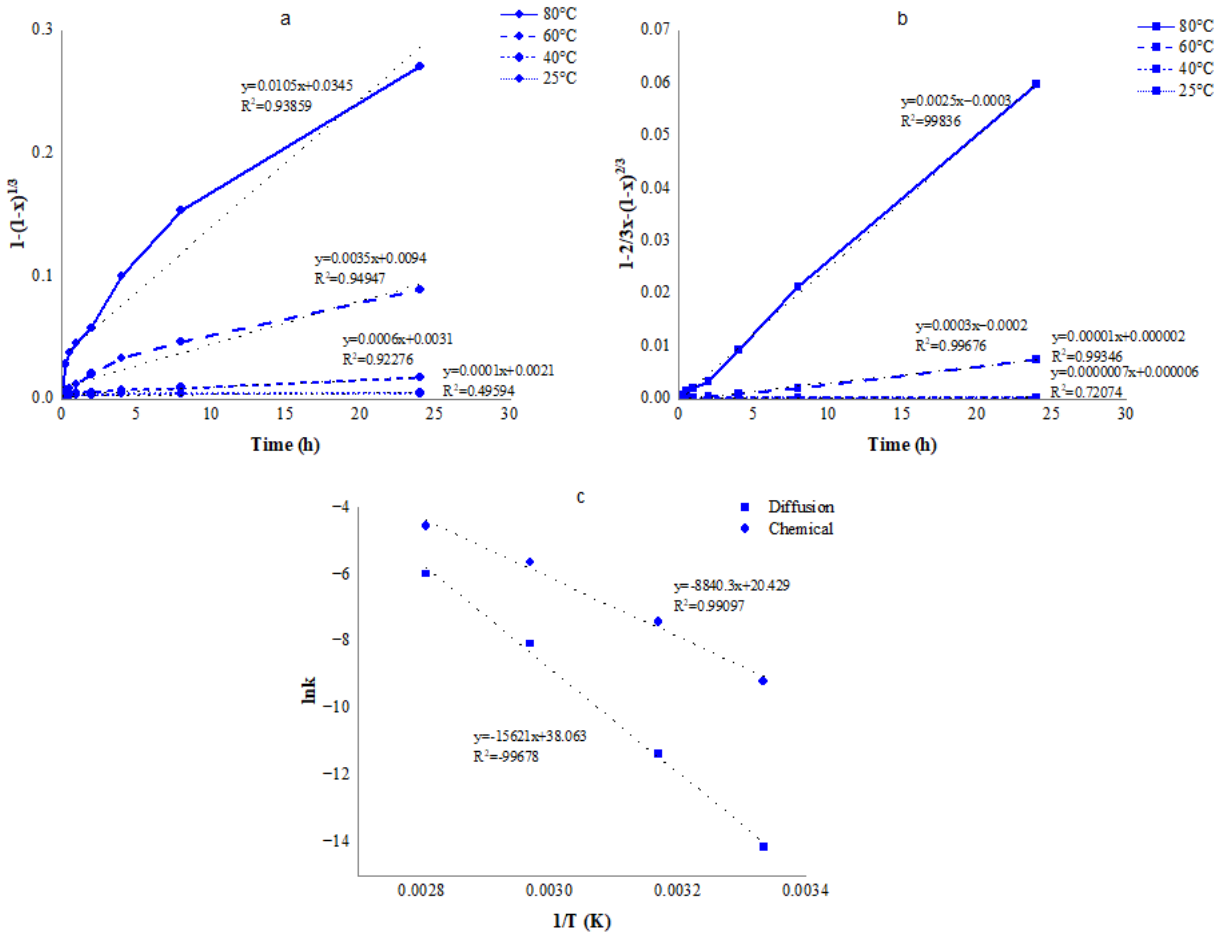

Figure 15: Plot of the shrinking core model for the leaching of sphalerite in ethaline with $CuCl_2$. (a) Plot of $1-(1-x)^{\frac{1}{3}}$ versus time at various temperatures. (b) Plot of $1-\frac{2}{3}x-(1-x)^{2/3}$ versus time at various temperatures. (c) Arrhenius plot of reaction rate against reciprocal of temperature.

Table 11 presents the coefficients of determination (R^2) for chemical reaction-controlled and diffusion-controlled kinetic models fitted to the leaching data of sphalerite in ethaline with $CuCl_2$. The data covers a range of temperatures (26°C, 40°C, 60°C, and 80°C) and different time intervals from the full reaction duration (0–24 h) down to the initial half hour (0–0.5 h). The R^2 values provide a statistical measure of how well each model fits the experimental data at each condition. Generally, higher R^2 values indicate a better model fit. Comparing these values across different time ranges and temperatures helps assess the validity and applicability of each kinetic model under varying experimental conditions.

Table 11: Coefficients of determination (R^2) for chemical and diffusion kinetic models for the leaching of sphalerite in Ethaline with $CuCl_2$ over various time ranges at different temperatures.

Time range (h)	26°C		40°C		60°C		80°C	
	Chemical	Diffusion	Chemical	Diffusion	Chemical	Diffusion	Chemical	Diffusion
0-24	0.4959	0.7207	0.9228	0.9935	0.9495	0.9968	0.9386	0.9984
0-8	0.6098	0.8448	0.791	0.9803	0.9479	0.9952	0.9559	0.9879
0-4	0.6618	0.9208	0.7213	0.9492	0.971	0.9792	0.9146	0.9686
0-2	0.5622	0.7749	0.692	0.9087	0.9424	0.9738	0.7652	0.961
0-1	0.6975	0.8713	0.783	0.9555	0.8652	0.9949	0.7997	0.9553
0-0.5	0.8183	0.8767	0.861	0.9398	0.9105	0.9878	0.9232	0.9943

Kinetic modeling of sphalerite leaching in Ethaline+$FeCl_3$ system

As illustrated in Figure 16a, the chemical reaction model $[1-(1-x)^{\frac{1}{3}}]$ fits the experimental data with relatively strong correlation coefficients, particularly at 40°C (R^2=0.9733) and 25°C (R^2=0.9543), indicating a significant role of surface reaction at lower to moderate temperatures. The leaching rate increased with temperature, as reflected in the steeper slopes at 80°C, though the linearity slightly diminished (R^2=0.9407).

On the other hand, the diffusion-controlled model $[1-\frac{2}{3}x-(1-x)^{2/3}]$, shown in Figure 16b, produced highly linear trends at elevated temperatures, with the best fit observed at 80°C (R^2=0.9992). This suggests that, under these conditions, the leaching process is increasingly governed by diffusion through the solid product layer. The results at 60°C and 40°C (R^2=0.9909 and 0.9834) further support this transition. As a result, the best fit for the experimental data was the diffusion control model.

Arrhenius plots (Figure 16c) were used to determine activation energies for both mechanisms. The calculated Ea values were 54.8 kJ/mol for the chemical model and 106.7 kJ/mol for the diffusion model. The higher Ea for diffusion implies a greater sensitivity to temperature and confirms that mass transport becomes the controlling step at higher temperatures.

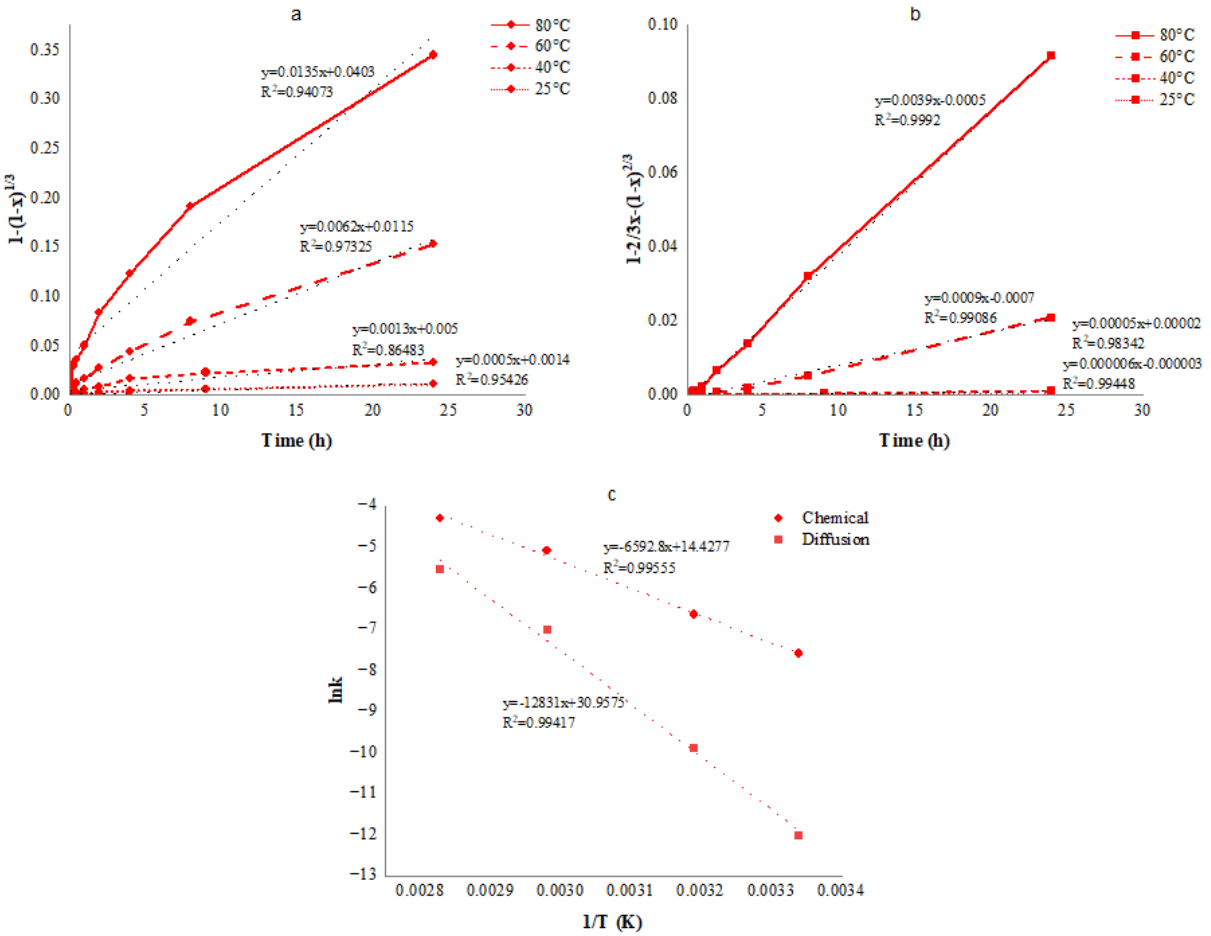

Figure 16: Plot of the shrinking core model for the leaching of sphalerite in ethaline with $FeCl_3$. (a) Plot of $1-(1-x)^{\frac{1}{3}}$ versus time at various temperatures. (b) Plot of $1-\frac{2}{3}x-(1-x)^{2/3}$ versus time at various temperatures. (c) Arrhenius plot of reaction rate against reciprocal of temperature.

Table 12 below presents the R^2 value, which shows quality of fit for each model in describing the leaching behavior of sphalerite in ethaline with $FeCl_3$ across various time intervals.

Table 12: Coefficients of determination (R^2) for chemical and diffusion kinetic models for the leaching of sphalerite in Ethaline with $FeCl_3$ over various time ranges at different temperatures.

Time (h)	26°C		40°C		60°C		80°C	
	Chemical	Diffusion	Chemical	Diffusion	Chemical	Diffusion	Chemical	Diffusion
24	0.9543	0.9945	0.8648	0.9834	0.9733	0.9909	0.9407	0.9992
8	0.9325	0.9945	0.9205	0.9814	0.9817	0.9763	0.9594	0.9992
4	0.9267	0.9945	0.9881	0.9521	0.9657	0.9878	0.9456	0.9992
2	0.8799	0.9945	0.9574	0.9893	0.9542	0.9851	0.9329	0.9992
1	0.8738	0.9945	0.955	0.9857	0.9288	0.9955	0.8467	0.9992
0.5	0.8317	0.9945	0.9578	0.9984	0.9831	0.9804	0.8785	0.9992

4.2 Leaching Results in Aqueous Medium

4.2.1 Effect of temperature on leaching

The leaching results show that temperature has a strong influence on zinc extraction from sphalerite in aqueous solutions. In both $FeCl_3$ and $CuCl_2$ systems, increasing the temperature generally accelerated the initial extraction rate. For $FeCl_3$, at 42.4°C, zinc extraction reached 68% after 24 hours, while at 61.7°C it was only around 40%, and at 81.4°C the extraction plateaued at about 38% after just 8 hours. Although higher temperatures promoted faster initial extraction, prolonged leaching led to a decrease or stagnation in extraction yield, likely due to surface passivation or precipitation phenomena that inhibit further zinc dissolution.

For $CuCl_2$ systems, a similar trend was observed: higher temperatures increased extraction rates slightly, but the overall zinc recovery remained much lower, not exceeding 12% after 8-24 hours even at 81.3°C.

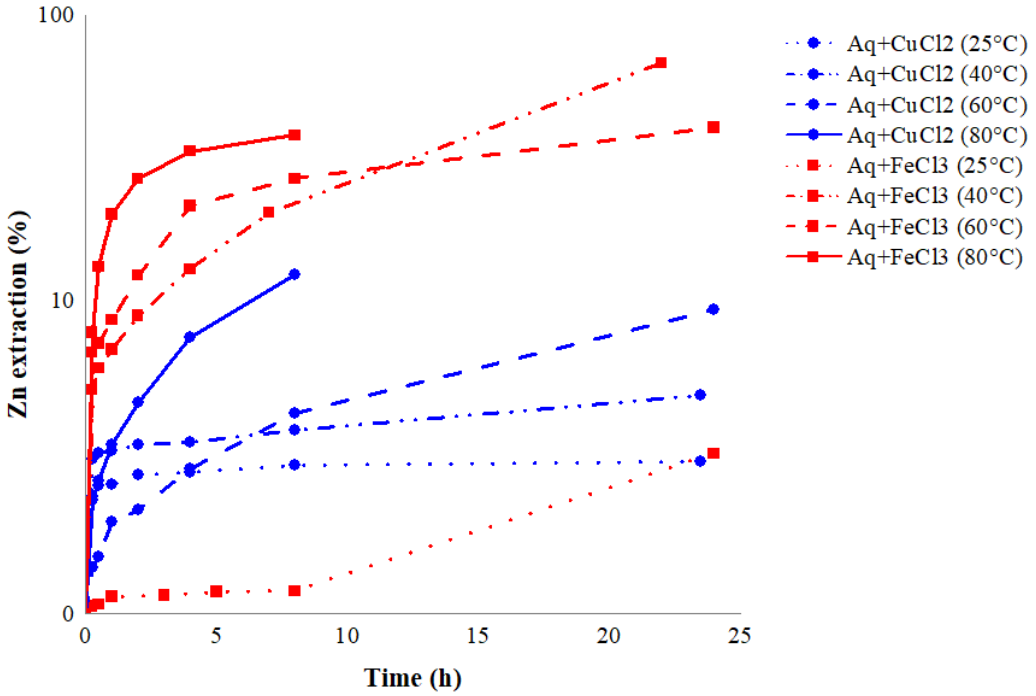

Figure 17: Effect of temperature and oxidants on zinc dissolution in aqueous media.

4.2.2 Effect of oxidants on leaching

The type of oxidant played a major role in determining the extent of zinc extraction. $FeCl_3$ was much more effective than $CuCl_2$ under identical conditions. In $FeCl_3$ solutions, zinc extraction reached significantly higher values across all temperatures, with up to 68% extraction at 42.4 °C after 24 hours, compared to less than 10% for $CuCl_2$ solutions over the same period. This can be attributed to the stronger oxidizing power of Fe^{3+} ions compared to Cu^{2+} ions when

attacking the sphalerite structure. Therefore, $FeCl_3$ proved to be a superior oxidant for sphalerite dissolution in aqueous solutions.

4.2.3 Kinetic analysis

Kinetic modeling of sphalerite leaching in Aqueous+$FeCl_3$ system

The kinetic modeling of sphalerite leaching in aqueous $FeCl_3$ (Figure 18) demonstrates that the process is predominantly diffusion-controlled at higher temperatures. The chemical reaction control model, represented by the plot of $1-(1-x)^{\frac{1}{3}}$ (Figure 18a), yields high R^2 values at lower temperatures, such as 0.9596 at 26°C and 0.9837 at 40°C, indicating good fits to surface-controlled kinetics in the early stages. However, the diffusion-controlled model $1-\frac{2}{3}x-(1-x)^{2/3}$ (Figure 18b) becomes more dominant as temperature increases, with a notable R^2=0.9892 at 60°C, and still strong at 0.9237 at 80°C, surpassing the chemical model's fit at these higher temperatures (0.8834 and 0.7822, respectively). This shift suggests a transition from chemical to diffusion control with increasing temperature, likely due to product layer formation slowing the leaching process.

Most importantly, the Arrhenius plot in Figure 18c yields an activation energy of 49 kJ/mol for the chemical reaction and a much higher 85.7 kJ/mol for diffusion. Since chemical control typically exhibits Ea>40 kJ/mol and diffusion control is characterized by Ea<20 kJ/mol, these values confirm that the rate-limiting step is the surface chemical reaction. Thus, $FeCl_3$ leaches sphalerite primarily through a chemically controlled mechanism that is strongly temperature dependent.

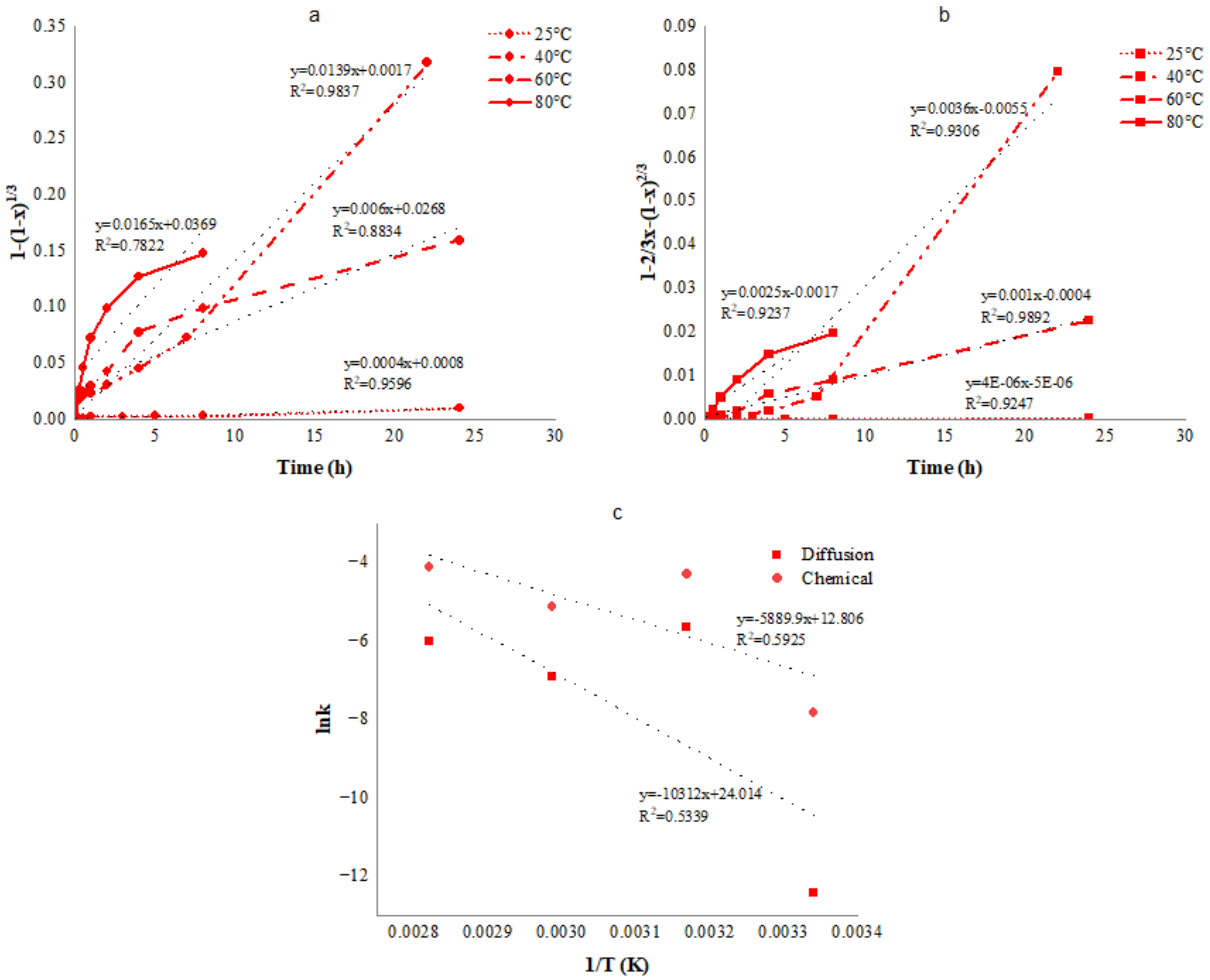

Figure 18: Plot of the shrinking core model for the leaching of sphalerite in aqueous with $FeCl_3$. (a) Plot of $1-(1-x)^{\frac{1}{3}}$ versus time at various temperatures. (b) Plot of $1-\frac{2}{3}x-(1-x)^{2/3}$ versus time at various temperatures. (c) Arrhenius plot of reaction rate against reciprocal of temperature.

Table 13: Coefficients of determination (R^2) for chemical and diffusion kinetic models for the leaching of sphalerite in Aqueous with $FeCl_3$ over various time ranges at different temperatures.

Time range (h)	26°C		40°C		60°C		80°C	
	Chemical	Diffusion	Chemical	Diffusion	Chemical	Diffusion	Chemical	Diffusion
0-24	0.9596	0.9247	0.9837	0.9306	0.8834	0.9892	0.7822	0.9237
0-8	0.6634	0.8217	0.9505	0.9579	0.9132	0.9779	0.7822	0.9237
0-4	0.6939	0.8483	0.8539	0.9883	0.9398	0.9528	0.8659	0.9801
0-2	0.6172	0.7147	0.7361	0.954	0.7891	0.9681	0.9203	0.9941
0-1	0.9487	0.9508	0.7164	0.8868	0.6894	0.8587	0.9699	0.9838
0-0.5	0.8711	0.9521	0.8679	0.9476	0.8042	0.8521	0.9923	0.9655

Kinetic modeling of sphalerite leaching in Aqueous+$CuCl_2$ system

The kinetic behavior of sphalerite leaching in aqueous $CuCl_2$ (Figure 19) is clearly controlled by surface chemical reactions, especially at elevated temperatures. The chemical model $1-(1-x)^{\frac{1}{3}}$, (Figure 19a) shows poor correlation at low temperatures, with $R^2 = 0.1861$ at 26°C and 0.441 at 40°C, but becomes strongly linear at 60°C (0.9811) and 80°C (0.9799). The diffusion-controlled model $1-\frac{2}{3}x-(1-x)^{2/3}$ (Figure 19b) improves with temperature as well, with $R^2 = 0.9727$ at 60°C and 0.9706 at 80°C, but remains consistently lower than or equal to the chemical model. Additionally, the activation energy values from the Arrhenius plot (Figure 19c) are 50.1 kJ/mol for the chemical reaction and 72 kJ/mol for diffusion — both well above the expected range for diffusion control. These findings strongly indicate that the rate-limiting step is the surface chemical reaction, particularly at higher temperatures, where temperature dependence becomes more significant. Unlike $FeCl_3$, the $CuCl_2$ system does not show a clear shift toward diffusion control, and chemical kinetics dominate across the observed range.

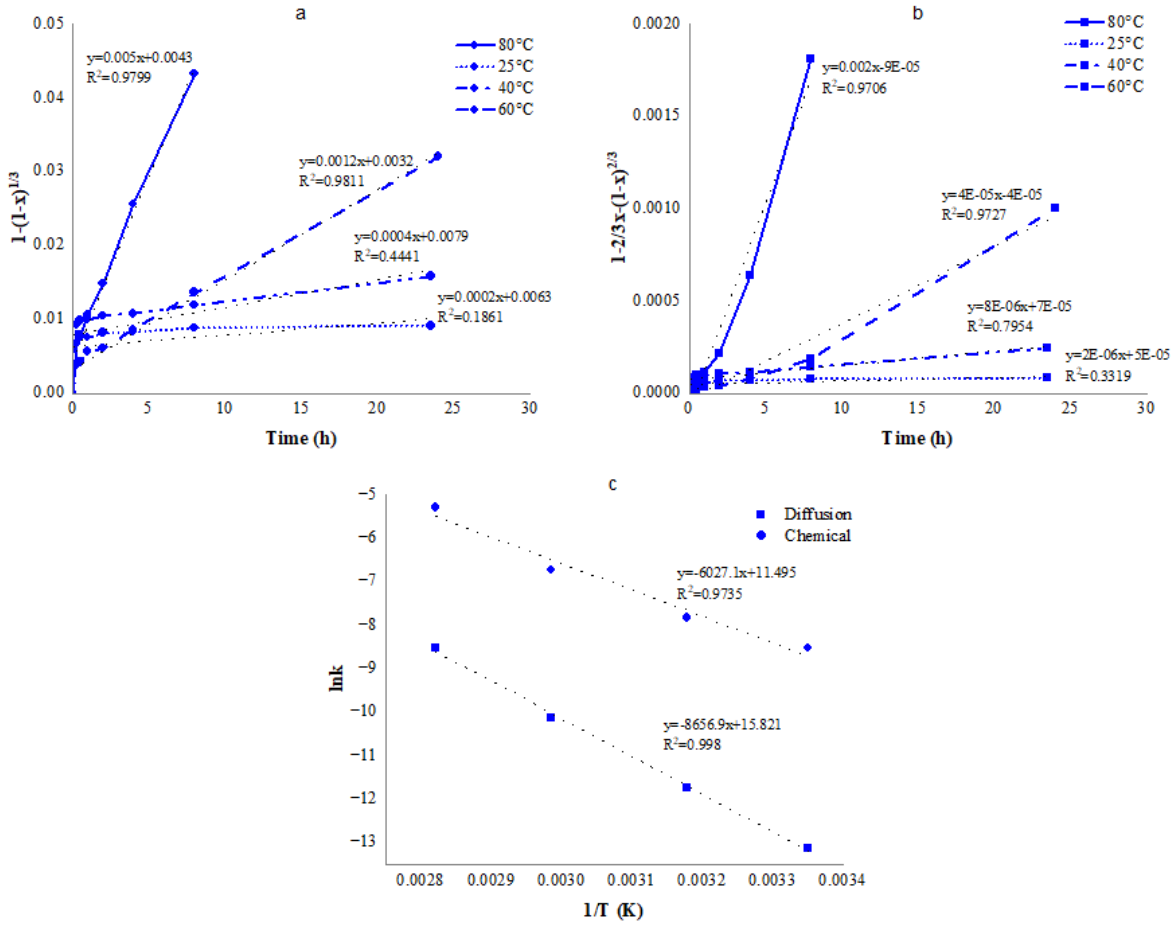

Figure 19: Plot of the shrinking core model for the leaching of sphalerite in aqueous with $CuCl_2$. (a) Plot of $1-(1-x)^{\frac{1}{3}}$ versus time at various temperatures. (b) Plot of $1-\frac{2}{3}x-(1-x)^{2/3}$ versus time at various temperatures. (c) Arrhenius plot of reaction rate against reciprocal of temperature.

Table 14: Coefficients of determination (R^2) for chemical and diffusion kinetic models for the leaching of sphalerite in Aqueous with $CuCl_2$ over various time ranges at different temperatures.

Time range (h)	26°C		40°C		60°C		80°C	
	Chemical	Diffusion	Chemical	Diffusion	Chemical	Diffusion	Chemical	Diffusion
0-24	0.1861	0.3319	0.441	0.7954	0.9811	0.9727	0.9799	0.9706
0-8	0.2627	0.422	0.2749	0.4987	0.8954	0.9794	0.9799	0.9706
0-4	0.3005	0.4285	0.2693	0.3687	0.7484	0.9591	0.9469	0.9699
0-2	0.4013	0.5212	0.3631	0.4473	0.6412	0.85	0.8471	0.9935
0-1	0.5409	0.6079	0.5187	0.5688	0.7688	0.9401	0.8114	0.9715
0-0.5	0.8155	0.8719	0.7863	0.8201	0.8134	0.8685	0.8536	0.9299

4.3 Comparison of Sphalerite Leaching in Different Media

Table 15 summarizes the calculated activation energies (Ea) for both chemical reaction-controlled and diffusion-controlled kinetic models across different media—ethaline with $FeCl_3$, ethaline with $CuCl_2$, aqueous $FeCl_3$, and aqueous $CuCl_2$—over a range of time intervals from 0.5 to 24 hours. The values were derived from Arrhenius plots corresponding to each model. The final column indicates the inferred rate-controlling step based on comparison of the activation energies, where values above ~40 kJ/mol typically suggest a chemically controlled process and values below ~20 kJ/mol are indicative of diffusion control.

For most cases, particularly in ethaline-based systems and aqueous $FeCl_3$, the activation energy values remain consistently high for both models, supporting a chemical reaction-controlled mechanism. However, in the aqueous $CuCl_2$ system, the activation energy significantly drops during the earlier stages (0.5–2 h), indicating a possible shift toward diffusion-controlled behavior at shorter reaction times.

Table 15: Summary of calculated activation energies (Ea) for chemical reaction-controlled and diffusion-controlled kinetic models in different media.

Media	**Time range (h)**	**Activation Energy (kJ/mol)**		**Rate Controlling step**
		Chemical	**Diffusion**	
Eth + FeCl3	0-24	54.8	106.7	Chemical-control
	0-8	57.6	104.2	Chemical-control
	0-4	53.4	101.4	Chemical-control
	0-2	54.4	103.4	Chemical-control
	0-1	51.3	103.4	Chemical-control
	0-0.5	53.2	103.4	Chemical-control

Eth + CuCl2	0-24	73.5	129.9	Chemical-control
	0-8	61.5	117.3	Chemical-control
	0-4	56.3	108.9	Chemical-control
	0-2	50.2	101.4	Chemical-control
	0-1	45.6	88.6	Chemical-control
	0-0.5	44	85	Chemical-control
Aq+FeCl3	0-24	49	85.7	Chemical-control
	0-8	58.5	107.8	Chemical-control
	0-4	64.2	122.9	Chemical-control
	0-2	64	124.2	Chemical-control
	0-1	52.7	104.4	Chemical-control
	0-0.5	54.4	105.2	Chemical-control
Aq+CuCl2	0-24	50.1	72	Chemical-control
	0-8	35.3	42.4	Mixed-control
	0-4	22.2	41.4	Mixed-control
	0-2	9.9	18.8	Diffusion controlled
	0-1	3	4.6	Diffusion controlled
	0-0.5	3.8	8.2	Diffusion controlled

The comparative Zn extraction shown in the Figure 20 illustrate the influence of oxidant type-$FeCl_3$ versus $CuCl_2$-on leaching performance in both aqueous and ethaline media at varying temperatures. At low temperatures (25°C and 40°C; a and b), $FeCl_3$ consistently outperforms $CuCl_2$ in aqueous solution, with Zn extraction reaching around 3.5% at 25°C and approximately 68% at 40°C for $FeCl_3$, compared to much lower values with $CuCl_2$ under the same conditions. This trend persists at 60°C (c), where aqueous $FeCl_3$ yields nearly 41% Zn extraction, significantly higher than aqueous $CuCl_2$ (9%). However, in ethaline media, $FeCl_3$ demonstrates enhanced reactivity at higher temperatures. At 80°C (Figure d), ethaline-$FeCl_3$ surpasses all other systems, achieving over 72% Zn extraction, followed closely by ethaline-$CuCl_2$ (61%). These results clearly demonstrate that $FeCl_3$ is the more effective oxidant overall, regardless of solvent type or temperature. Its higher oxidative potential and consistent performance across all experimental conditions suggest it is more suitable for sphalerite leaching than $CuCl_2$. This highlights the dominant role of $FeCl_3$ in both aqueous and ethanolic media, particularly when targeting high zinc recovery across a range of thermal conditions.

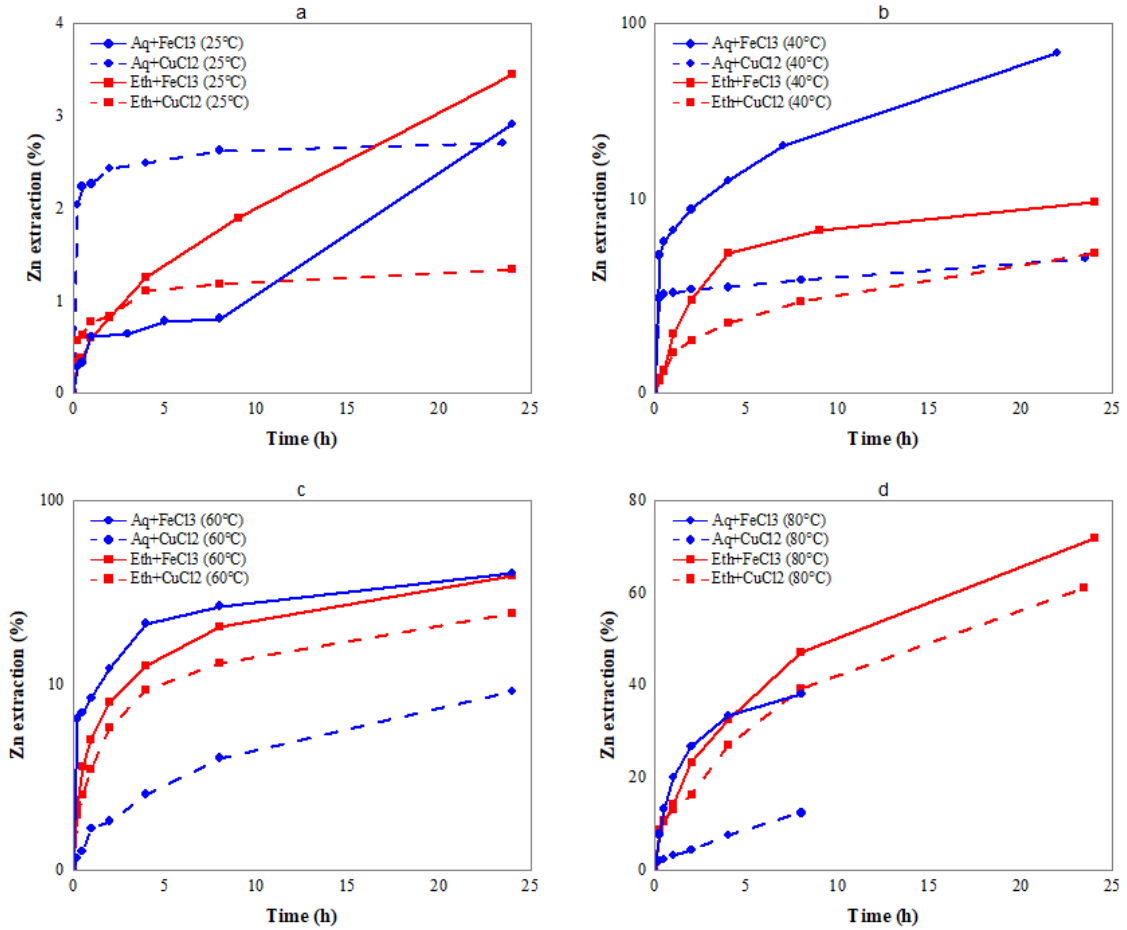

Figure 20: Effect of Oxidant Type ($FeCl_3$ vs $CuCl_2$) and Solvent Medium (Aqueous vs Ethaline) on Zn Extraction from Sphalerite at Different Temperatures: (a) 25°C, (b) 40°C, (c) 60°C, and (d) 80°C.

Table 16 presents the leaching results of sphalerite in different media at varying temperatures. It is evident that systems containing $FeCl_3$ as an oxidizing agent yielded higher zinc extraction efficiencies. For instance, the extraction percentage in the aqueous + $FeCl_3$ system at 40°C reached 68.3%, which is unexpectedly higher than the value obtained at 60°C, suggesting possible experimental error. The aqueous system at 80°C was conducted for a maximum of 8 hours due to evaporation issues. Furthermore, zinc extraction was generally higher in ethaline-based media compared to aqueous solutions. Among the variables studied, temperature and the presence of oxidants were observed to have a significant influence on leaching performance.

Table 16: Zn extraction from sphalerite of different systems at different temperatures after 24 hours.

System	T (°C)			
	25°C	40°C	60°C	80°C
Aq+FeCl3	2.9%	68.3%	40.6%	38.1% (8 hour)
Aq+CuCl2	2.7%	4.7%	9.3%	12.4% (8 hour)
Eth+FeCl3	3.5%	9.7%	39.3%	71.9%
Eth+CuCl2	1.3%	5.0%	24.4%	61.1%

Based on the data presented in the table below, the diffusion-controlled kinetic model provided the best fit across all experimental conditions. This suggests that subsequent calculations of activation energy (Ea) should be based on this model. According to the shrinking core model theory, when the extraction behavior follows the equation $\left(1-\frac{2}{3}x-(1-x)^{\frac{2}{3}}\right)$, the process is governed by internal diffusion. In contrast, if the data aligns with the expression $(1-(1-x)^{\frac{1}{3}})$, the rate-controlling step is the surface chemical reaction. In this study, the experimental results were consistent with the inner diffusion model, confirming that diffusion was the dominant rate-controlling mechanism. However, a comparison with activation energy values presents a more nuanced interpretation. Literature indicates that a system is considered diffusion-controlled when Ea is less than 20 kJ/mol, chemically controlled when Ea exceeds 40 kJ/mol, and mixed-controlled when Ea lies between 20 and 40 kJ/mol. Interestingly, the calculated activation energies in this study ranged from 49 to 73.5 kJ/mol, placing all systems firmly in the chemically controlled regime. This apparent contradiction suggests that, while the kinetic model indicates a diffusion-controlled mechanism, the relatively high activation energies imply that surface chemical reactions may still play a significant role, or that the overall process is more complex than a single rate-controlling step.

Moreover, the activation energies for leaching with $CuCl_2$ as an oxidant were consistently higher than those for $FeCl_3$-based systems, both in aqueous and ethaline media. This trend correlates with the observed lower zinc extraction values in the $CuCl_2$ systems. Higher activation energy generally indicates a slower reaction rate or a higher energy barrier for the leaching process. Therefore, the lower zinc conversion in $CuCl_2$ media can be attributed to the greater energy required to initiate and sustain the reaction compared to $FeCl_3$.

Among all tested systems, leaching in the presence of ferric ions ($FeCl_3$) resulted in the highest zinc extraction. This can be attributed to the strong oxidizing potential of Fe^{3+}, which more effectively promotes the oxidation of sphalerite and facilitates zinc dissolution. Additionally, ferric ions are known to react more favorably with sulfide minerals, accelerating the breakdown of the ZnS matrix and enhancing metal recovery.

Table 17: Summarized result of the kinetic analysis.

System	R^2 (Chemical)	R^2 (Diffusion)	Ea (Diffusion), kJ/mol	Ea (Chemical), kJ/mol	X, %
Aq+FeCl3	0.7822	**0.9237**	49	85.7	38.1
Aq+CuCl2	**0.9799**	0.9706	50.1	72	12.4
Eth+FeCl3	0.9407	**0.9992**	54.8	106.7	71.9
Eth+CuCl2	0.9386	**0.9984**	73.5	129.9	61.1

CHAPTED FIVE: SUMMARY AND CONCLUSION

This study systematically examined the leaching behavior of sphalerite in two different solvent systems—ethaline (a deep eutectic solvent) and aqueous media—using $FeCl_3$ and $CuCl_2$ as oxidizing agents. The leaching performance was evaluated under varying temperature conditions to determine the influence of these variables on zinc extraction efficiency and reaction kinetics.

The results demonstrated that zinc extraction was significantly affected by the nature of the oxidant, the choice of solvent medium, and the leaching temperature. Among all the tested conditions, the highest zinc recovery (approximately 72%) was achieved using $FeCl_3$ in ethaline at 80°C, underscoring the strong oxidative capability of Fe^{3+} ions and the effectiveness of DESs as alternative leaching media at elevated temperatures. In contrast, $CuCl_2$-based systems generally resulted in lower zinc extraction, which was attributed to their higher activation energy requirements, reflecting slower leaching kinetics.

Kinetic modeling using the shrinking core model indicated that, in all systems, the experimental data were best described by the diffusion-controlled model. This was supported by high R^2 values—frequently exceeding 0.95 in $FeCl_3$ systems—indicating a good correlation between the experimental results and the model. The kinetic equations suggested that internal diffusion was the dominant mechanism for the leaching process. However, a detailed analysis of the apparent activation energies introduced complexity to this interpretation. The calculated activation energies for all systems ranged from 49 to 73.5 kJ/mol, values which fall within the range typically associated with chemically controlled reactions.

According to the literature, activation energies below 20 kJ/mol indicate diffusion-controlled processes, whereas values above 40 kJ/mol suggest chemical reaction control. The relatively high activation energies obtained in this study thus suggest that, despite the kinetic model's fit, the rate-controlling step might actually be surface chemical reaction or a mixed control mechanism. This highlights the possibility of multiple overlapping processes influencing the overall reaction rate.

Furthermore, the $FeCl_3$ systems—both aqueous and ethaline—not only showed higher zinc extraction rates but also lower activation energy values than the $CuCl_2$ systems. This confirms the superior efficiency of Fe^{3+} as an oxidant in the leaching of sphalerite, likely due to its greater redox potential and enhanced interaction with the sulfide matrix.

In summary, this research confirms that deep eutectic solvents like ethaline, particularly when combined with a strong oxidizing agent such as $FeCl_3$, offer promising potential for the leaching of sphalerite. The study also underscores the importance of considering both kinetic model fitting and activation energy data for a comprehensive understanding of leaching mechanisms. Future work should explore more detailed mechanistic studies and process optimization to fully harness the benefits of DESs in hydrometallurgical applications.

Literature Cited

1. Bidari E, Winardhi CW, Da Godinho JRA, Frisch G. Role of Oxidants in Metal Extraction from Sulfide Minerals in a Deep Eutectic Solvent. ACS Omega 2024; 9(12):14592–603.

2. Sokić MD, Bugarčić M, Jovanović AA. Sphalerite Leaching in Acid Media: a Review. Metall Mater Data 2023; 1(2):33–43.

3. International Zinc Association. Zinc College: Course Notes 2002.

4. Cao L, Huang S, Shulin E. ZnS/CdS/ZnS quantum dot quantum well produced in inverted micelles. J Colloid Interface Sci 2004; 273(2):478–82.

5. Introduction to Zinc.

6. Richter J, Ruck M. Ionometallurgy: an academic exercise or promising approach? RSC Sustainability 2024; 2(5):1202–14.

7. Karimi S, Rashchi F, Moghaddam J. Parameters optimization and kinetics of direct atmospheric leaching of Angouran sphalerite. International Journal of Mineral Processing 2017; 162:58–68.

8. Abbott AP, Frisch G, Gurman SJ, Hillman AR, Hartley J, Holyoak F et al. Ionometallurgy: designer redox properties for metal processing. Chem Commun (Camb) 2011; 47(36):10031–3.

9. Smith EL, Abbott AP, Ryder KS. Deep eutectic solvents (DESs) and their applications. Chem Rev 2014; 114(21):11060–82.

10. Hansen BB, Spittle S, Chen B, Poe D, Zhang Y, Klein JM et al. Deep Eutectic Solvents: A Review of Fundamentals and Applications. Chem Rev 2021; 121(3):1232–85.

11. Zinc Metal | AMERICAN ELEMENTS®; 2025 [cited 2025 Apr 17]. Available from: URL: https://www.americanelements.com/zinc-metal-7440-66-6.

12. Sphalerite: The primary ore of zinc and a collector's gem; 2025 [cited 2025 Apr 22]. Available from: URL: https://geology.com/minerals/sphalerite.shtml.

13. Sphalerite: Mineral information, data and localities; 2025 [cited 2025 Apr 22]. Available from: https://www.mindat.org/min-3727.html

14. Sphalerite: Physical and optical properties, occurrence, uses & more; 2025 [cited 2025 Apr 22]. Available from: https://geologyscience.com/minerals/sphalerite/

15. Sphalerite. Wikipedia; 2025 [cited 2025 Apr 22]. Available from: https://en.wikipedia.org/wiki/Sphalerite.

16. Zinc smelting - Wikipedia; 2025 [cited 2025 May 2]. Available from: URL: https://en.wikipedia.org/wiki/Zinc_smelting.

17. Huang H-H. The Eh-pH Diagram and Its Advances. Metals 2016; 6(1):23.

18. Larsen DM, Linkson PB. Thermodynamics of the zinc-sulfur dioxide-water system. Metall Trans B 1993; 24(3):409–17.

19. Souza AD, Pina PS, Leão VA, Silva CA, Siqueira PF. The leaching kinetics of a zinc sulphide concentrate in acid ferric sulphate. Hydrometallurgy 2007; 89(1-2):72–81.

20. Nnanwube IA, Udeaja JN, Onukwuli OD. Kinetics of zinc recovery from sphalerite in acetic acid solution 2020.

21. Crundwell FK, Verbaan B. Kinetics and Mechanisms of the Non-oxidative Dissolution of Sphalerite (Zinc Sulphide) 1986.

22. Crundwell FK. Kinetics and Mechanism of the Oxidative Dissolution of a Zinc Sulphide Concentrate in Ferric Sulphate Solutions 1987.

23. Picazo-Rodríguez NG, Soria-Aguilar MdJ, Martínez-Luévanos A, Almaguer-Guzmán I, Chaidez-Félix J, Carrillo-Pedroza FR. Direct Acid Leaching of Sphalerite: An Approach Comparative and Kinetics Analysis. Minerals 2020; 10(4):359.

24. Jenkin GR, Al-Bassam AZ, Harris RC, Abbott AP, Smith DJ, Holwell DA et al. The application of deep eutectic solvent ionic liquids for environmentally-friendly dissolution and recovery of precious metals. Minerals Engineering 2016; 87:18–24.

25. Shahrezaei F, Karimi S, Behnajady B. Experimental and dynamic molecular study of zinc extraction from sphalerite concentrate in ternary deep eutectic solvent. Colloids and Surfaces A: Physicochemical and Engineering Aspects 2024; 695:134241.

26. Winardhi CW, Da Godinho JRA, Rachmawati C, Achin ID, Iturbe AU, Frisch G et al. A particle-based approach to predict the success and selectivity of leaching processes using ethaline - Comparison of simulated and experimental results. Hydrometallurgy 2022; 211:105869.

27. H. Scott Fogler. Elements of Chemical Reaction Engineering. 3rd edition; 1999.

28. Levenspiel O. Chemical Reaction Engineering: 3rd Edition. 3rd Edition. John Wiley & Sons; 1999. (3rd Edition).

29. Michael L. Free. Hydrometallurgy: Fundamentals and Applications. John Wiley & Sons, Inc., Hoboken, New Jersey; 2013.

30. YAN X, ZHUANG H, WANG Y, WANG X, ZHANG Z, YANG L. Kinetics and Mechanism on Removal of Aluminum from Phosphoric Medium by Solvent Extraction using Lewis Cells. SERDJ 2021; 28(1):95–108.

31. Lasaga AC. Kinetic Theory in the Earth Sciences. Princeton University Press; 1998.

32. Chemistry LibreTexts. 6.2.3.4: The Arrhenius Law - Arrhenius Plots; 2013 [cited 2025 May 2]. Available from: URL: https://chem.libretexts.org/Bookshelves/Physical_and_Theoretical_Chemistry_Textbook_Maps/Supplemental_Modules_%28Physical_and_Theoretical_Chemistry%29/Kinetics/06%3A_Modeling_Reaction_Kinetics/6.02%3A_Temperature_Dependence_of_Reaction_Rates/6.2.03%3A_The_Arrhenius_Law/6.2.3.04%3A_The_Arrhenius_Law_-_Arrhenius_Plots.